

Graphical Abstract

A Radiation Exchange Factor Transformation with Proven Convergence, Non-Negativity, and Energy Conservation

Nikolaj Maack Bielefeld

Highlights

A Radiation Exchange Factor Transformation with Proven Convergence, Non-Negativity, and Energy Conservation

Nikolaj Maack Bielefeld

- A matrix-based exchange factor transformation for multiple reflection-scattering radiative transfer on general domains
- Proven convergence bounds derived from reflection-scattering coefficients, domain discretization, and machine precision
- Guaranteed physically correct non-negative radiation to machine precision for non-negative source terms
- Exact energy conservation to machine precision under specified conditions
- Identification of a discrepancy in Noble's formulation of Hottel's zonal method for intermediate scattering albedos, which the proposed transformation avoids

A Radiation Exchange Factor Transformation with Proven Convergence, Non-Negativity, and Energy Conservation

Nikolaj Maack Bielefeld*

Independent researcher, Karl Bjarnhofs Vej 1A, st 2, 7120, Vejle East, Southern Jutland, Denmark

Abstract

This paper presents a matrix-based exchange factor transformation for solving coupled mixed boundary condition radiative transfer problems on general domains. The method applies to participating media ranging from transparent to absorbing, emitting, and scattering, with boundaries ranging from absorbing to reflecting. Given a first-interaction exchange factor matrix \mathbf{F} , the transformation produces an absorption matrix \mathbf{A} and a multiple reflection-scattering matrix \mathbf{R} through a Neumann series that analytically traces all reflection-scattering paths to steady state. The paper establishes rigorous conditions under which the method guarantees convergence, non-negative radiation, and exact energy conservation to machine precision. A comparison with Noble's matrix formulation of Hottel's zonal method reveals a previously unidentified discrepancy in that classical approach; the proposed transformation eliminates this discrepancy. The method is validated against the diffusion approximation in the high-extinction limit and against results of Crosbie and Schrenker for pure and partial scattering cases. The method is applicable to medium-scale general reflecting-scattering problems and scales to large problems when negligible reflection-scattering and high extinction ensure matrix sparsity.

Keywords: RTE, Radiative transfer, Exchange factors, Zonal method, Multiple scattering, Neumann series, Energy conservation, Matrix methods

1. Introduction

Radiative transfer in participating media is a fundamental process in many natural and engineered systems, from stellar atmospheres to thermal engineering. The theoretical foundation for radiative transfer was established in the 19th century by Gustav Kirchhoff, who formulated the fundamental relationship between emission and absorption of thermal radiation and introduced the concept of blackbody radiation [1]. Building upon this work, Karl Schwarzschild developed early formulations for radiative transfer in stellar atmospheres in the early 1900s [2]. The modern mathematical framework of the radiative transfer equation (RTE) was systematically developed by Subrahmanyan Chandrasekhar in his seminal 1950 treatise "Radiative Transfer" [3], which

*Corresponding author

Email address: nikolajbielefeld@gmail.com (Nikolaj Maack Bielefeld)

URL: <https://gert.net> (Nikolaj Maack Bielefeld)

provided rigorous analytical methods and established the equation as the cornerstone of radiation transport theory across diverse fields from astrophysics to engineering applications. Despite this rich theoretical heritage, the fundamental governing equation remains a challenging integro-differential equation in seven independent variables: Three spatial coordinates (x , y , z), two directional angles (θ , ϕ), one spectral wavelength (λ) and one temporal time (t). Under steady-state and grey media assumptions, the temporal (t) and spectral (λ) dependencies are eliminated, reducing the RTE from seven to five independent variables, which yields the differential form shown in equation (1) [4]:

$$\begin{aligned} \frac{\partial i(S, \Omega)}{\partial S} &= \kappa i_b(S) - \kappa i(S, \Omega) - \sigma_s i(S, \Omega) \\ &+ \frac{\sigma_s}{4\pi} \int_{\Omega_i=4\pi} i(S, \Omega_i) \Phi(\Omega_i, \Omega) d\Omega_i \end{aligned} \quad (1)$$

where $i(S, \Omega)$ is the intensity along a ray trajectory, as a function of position S and direction $\Omega \equiv \Omega(\theta, \phi)$, κ is the absorption coefficient of the medium, $i_b(S)$ is the blackbody intensity, σ_s is the scattering coefficient and Φ is the scattering phase function and the integral is over all solid angles (4π steradians).

The RTE of equation (1) is a differential energy balance along the trajectory S of a single ray. To solve it one could, in principle, simply integrate along the ray trajectory. What makes the RTE particularly challenging to solve for general geometries is that all possible ray trajectories in the domain are coupled through two mechanisms: (1) The state of the participating medium, i.e. the temperature of the intervening gas, which depends on the local radiative heating rate and governs both the rate of emission (through blackbody emission laws) and temperature-dependent absorption properties, and (2) the in-scattering term, which requires integration over all incoming directions to account for radiation scattered from every direction into the direction of S . Therefore, for general geometries, to determine the equilibrium state, all possible ray trajectories must be solved simultaneously, which explains why the RTE has historically resisted general analytical treatment, and is most commonly solved numerically, or through analytical solutions for special simplified cases [4].

As noted by Modest and Mazumder [5] in their most recent textbook:

"... to this day no truly satisfactory RTE solution method has emerged."
Modest and Mazumder, 2022.

The RTE does not directly account for surface reflections; the exchange factor transformation proposed in this paper provides a matrix framework for coupled reflection-scattering problems with proven convergence and energy conservation properties.

Seeking to quantify combustion heat transfer, Hottel and co-workers [6][7][8] pioneered solutions to the RTE using a discretized integral approach. Fundamentally, this integral approach produces matrices of *exchange areas*, which describe the radiative connectivity of the discretized domain. The integrals for the exchange areas are:

Surface-surface:

$$\overline{s_j s_k} = \frac{1}{\pi} \int_{A_j} \int_{A_k} \frac{\bar{i}(S_{j-k}) \cos(\theta_j) \cos(\theta_k)}{S_{j-k}^2} dA_k dA_j \quad (2)$$

Surface-gas and gas-surface:

$$\overline{s_k g_\gamma} = \overline{g_\gamma s_k} = \frac{\kappa}{\pi} \int_{V_\gamma} \int_{A_k} \frac{\bar{t}(S_{k-\gamma}) \cos(\theta_k)}{S_{k-\gamma}^2} dA_k dV_\gamma \quad (3)$$

Gas-gas:

$$\overline{g_\gamma g_{\gamma*}} = \frac{\kappa^2}{\pi} \int_{V_\gamma} \int_{V_{\gamma*}} \frac{\bar{t}(S_{\gamma-\gamma*})}{S_{\gamma-\gamma*}^2} dV_{\gamma*} dV_\gamma \quad (4)$$

where $\bar{t} = \exp(-\kappa S)$ is the transmissivity of the participating medium, θ is the angle with the surface normal, $\cos(\theta)$ of the emitter surface accounts for the diffuse Lambertian emission and $\cos(\theta)$ of the absorbing surface accounts for the projected area effect, S is the distance from the point of emission to the point of absorption and κ is the absorption coefficient of the medium. These integrals, being analytically intractable, were initially, before the general advent of modern-day digital computers, solved graphically and tabulated. Once the exchange areas have been determined for all pairs of emitters and absorbers in the system, subsequent solution of the RTE is achieved using linear algebra.

Prior to this period, having access to some of the first digital computers, Stanislav Ulam and co-workers pioneered the Monte Carlo method [9], a statistical method that can model complex phenomena which are analytically intractable. Not surprisingly, Monte Carlo methods can be applied to solve the multi-dimensional integrals formulated by Hottel and co-workers. A comprehensive review of radiative transfer methods can be found in [4] and [5].

Similarly to Hottel's method, outlined above, the exchange factor transformation of the present work starts from the exchange area matrix. But unlike Hottel's method, which works directly with the exchange area matrix, the proposed transformation uses its non-dimensional counterpart, the *exchange factor* matrix, where each row of the exchange area matrix has been normalized by its equivalent area of emission. Before solving a specific problem, the proposed method applies a matrix transformation to augment the exchange factor matrix with additional information about the steady state of reflection and scattering in the domain.

The transformation of the exchange factor matrix into an augmented form is partly inspired by the "F-hat" method developed by Beckman [10], which extends the view factor matrix for a transparent enclosure to include reflections. Further analysis revealed that the "F-hat" method only includes single reflections and does not account for multiple reflections. The effective reflection-scattering coefficients of multiple reflection-scattering processes on general domains are functions of extinction and geometry, which complicates their determination. However, by expressing the multiple reflection-scattering paths as a Neumann series, the steady-state solution can be obtained through matrix operations with guaranteed convergence under specified conditions.

Given the availability of an analytically derived matrix of exchange factors, generally referred to as the matrix \mathbf{F} , the entire solution is analytical. Thanks to Narayanaswamy [11], who found a general analytical solution to equation (2) with $\bar{t}(S) = 1$, this is possible for any convex enclosure composed of polygon surfaces and a transparent medium, giving perfect solutions to multiple reflection systems, which would otherwise be represented by coupled Fredholm equations of the second kind [12], the single assumption being that angular distributions of emission and reflection are identical.

For problems involving participating media ($\bar{t}(S) < 1$), analytical solutions to the multi-dimensional integrals of equations (2)-(4) have yet to be found. In this case, one might employ

Monte Carlo methods to obtain near-analytical estimates of \mathbf{F} . To ensure that \mathbf{F} satisfies both energy conservation and reciprocity, smoothing should be employed, such as for example the method proposed by Daun et al. [13].

The solution method proposed in this work is general and, furthermore, it is flexible. In fact, a key strength of exchange factor-based methods for solution of the RTE, is that they allow the formidable monolithic problem of energy transfer by an electromagnetic wave field, to be broken down into two conceptually separate and more manageable parts: The geometry and extinction-based ray propagation part and the system-wide energy interaction part. If \mathbf{F} is obtained through Monte Carlo ray tracing methods, any number of relevant optical phenomena may be modelled, such as refraction and diffraction, refraction being significant in atmospheric research, due to the variable refractive index. This can be achieved by solving differential equations for each ray [14]. Since the proposed transformation records only ray trajectory endpoints, it is in some sense blind to the phenomena which govern the trajectories, which explains why the matrix transformations of the present work will preserve any modelled ray trajectory properties.

For the proposed transformation, since \mathbf{F} refers only to the first interaction, Monte Carlo methods used to obtain \mathbf{F} can be truncated after this initial interaction, making them computationally less demanding than basic Monte Carlo implementations that must track multiple reflection-scattering events [15]. This will be increasingly true for higher single reflection-scattering coefficients due to the increased length of the ray paths. Instead, the proposed transformation performs the multiple reflection-scattering ray tracing analytically using solution of linear systems. This approach offers key advantages: (1) it can significantly improve computational efficiency compared to basic ray tracing methods for multiple reflection-scattering, (2) it provides analytical ray tracing accuracy with quantifiable bounds on the necessary numerical precision, (3) the precision requirements are expressed as a function of both the geometry and extinction (described by \mathbf{F}) and the reflection and scattering properties of each element. This enables problem-specific numerical precision tuning which is readily implementable in modern numerical programming languages [16].

The main novel contributions of this paper are: (1) a matrix transformation that converts first-interaction exchange factors into absorption and multiple reflection-scattering matrices via analytical path tracing, (2) rigorous proofs of convergence, non-negativity, and energy conservation under specified conditions, and (3) identification of a previously unreported discrepancy in Noble's formulation of Hottel's zonal method, which the proposed transformation avoids.

The remainder of the paper is structured as follows: Section 2 presents the methodology. Section 3 provides two theorems with proofs that rigorously establish the necessary convergence conditions. Section 4 presents theorems and proofs establishing the matrix properties used to guarantee physical correctness. Section 5 establishes physical correctness through guaranteed exact non-negative radiation and energy conservation to machine precision. Section 6 validates the transformation numerically by comparing its solutions to existing methods and demonstrates wide applicability. Section 7 discusses scalability, computational complexity, comparison to existing methods, limitations, and future work. Finally, Section 8 presents the conclusion.

2. Methodology

The methodology is split into three parts: First, the exchange factor matrix is formally defined, next, the exchange factor transformation is defined, and lastly, the transformed exchange factors are applied to solution of the RTE.

2.1. Definition of the Exchange Factor Matrix

The proposed transformation requires as an input a general description of the radiative connectivity of the domain in the form of the exchange factor matrix \mathbf{F} . The exchange factor matrix \mathbf{F} may be obtained analytically or numerically. All of the subsequent operations of the proposed transformation are analytical. The $(m+n) \times (m+n)$ row-stochastic blocked first interaction exchange factor matrix \mathbf{F} for a system of m bounding surfaces and n gas volume elements is defined as:

$$\mathbf{F} = \begin{bmatrix} \mathbf{F}_{ss} & \mathbf{F}_{sg} \\ \mathbf{F}_{gs} & \mathbf{F}_{gg} \end{bmatrix} \quad (5)$$

where \mathbf{F} is row stochastic to ensure that conservation of energy is satisfied and the entries of \mathbf{F} are the fractions of energy emitted by the emitter of row i which has its first interaction with the element of column j . The entries of \mathbf{F} can be defined from equations (2)-(4) by normalizing with the equivalent total capacity for emission and reflection-scattering of the emitter zone (and using the extinction coefficient β in place of the absorption coefficient κ):

$$F_{s_j s_k} = \frac{\overline{s_j s_k}}{(\rho_j + \varepsilon_j)A_j}, \quad F_{s_k g_\gamma} = \frac{\overline{s_k g_\gamma}}{(\rho_k + \varepsilon_k)A_k}, \quad F_{g_\gamma s_k} = \frac{\overline{g_\gamma s_k}}{4\beta V_\gamma}, \quad F_{g_\gamma g_{\gamma^*}} = \frac{\overline{g_\gamma g_{\gamma^*}}}{4\beta V_\gamma}. \quad (6)$$

where $\rho + \varepsilon = 1$ with ρ being the single reflectivity and ε is the emissivity and for volumes of participating media, $\kappa + \sigma_s = \beta$ where σ_s is the single scattering coefficient. This normalization ensures \mathbf{F} captures all outgoing radiation, whether emitted or reflected-scattered. Additionally, \mathbf{F} satisfies reciprocity [13]:

$$\mathbf{E}\mathbf{F} = \mathbf{F}^T\mathbf{E} \quad (7)$$

where \mathbf{E} is a diagonal matrix of equivalent emission areas with $\mathbf{E}_{ii} = (\rho_i + \varepsilon_i)A_i$ for $i \leq m$ and $\mathbf{E}_{ii} = 4\beta_i V_i$ for $i > m$, where the full capacity to emit and reflect-scatter is used.

Furthermore, in the general case, \mathbf{F} will have some zero entries, i.e., physical elements without direct view of each other, meaning \mathbf{F} is not merely a positive matrix but a non-negative matrix. Therefore, for the proofs of this paper to guarantee convergence, \mathbf{F} must be *irreducible* (strongly connected) [18], where irreducibility corresponds to the physical requirement that the domain contains no isolated regions, that is, for any two elements i and j , there exists a sequence of direct radiation exchanges $i \rightarrow k_1 \rightarrow k_2 \rightarrow \dots \rightarrow j$ connecting them. This requirement can always be satisfied by treating isolated regions as separate radiative transfer problems.

For the present transformation, \mathbf{F} should be derived exactly as if dealing with pure absorption, but always using the total capacity to emit and reflect-scatter instead of the absorption coefficient. Then after \mathbf{F} has been obtained, any part of the capacity to absorb may be converted into a capacity for reflection-scattering elementwise: A single \mathbf{F} covers all combinations of $\kappa_i + \sigma_{s,i}$ which sum to β_i , since grey radiation carries no information about its origin.

2.2. The Exchange Factor Transformation

The column constant $(m+n) \times (m+n)$ blocked single reflection-scattering matrix \mathbf{B} is defined as:

$$\mathbf{B} = \begin{bmatrix} \mathbf{B}_{ss} & \mathbf{B}_{sg} \\ \mathbf{B}_{gs} & \mathbf{B}_{gg} \end{bmatrix} = \begin{bmatrix} \rho_1 & \dots & \rho_m & \omega_1 & \dots & \omega_n \\ \vdots & \ddots & \vdots & \vdots & \ddots & \vdots \\ \rho_1 & \dots & \rho_m & \omega_1 & \dots & \omega_n \end{bmatrix} \quad (8)$$

where ρ_i is the reflectivity of boundary element i and $\omega_i = \sigma_{s,i}/\beta_i$ is the single scattering albedo of volume element i . The single reflection-scattering interaction matrix \mathbf{K} and the steady state path matrix \mathbf{S}_∞ are defined as:

$$\mathbf{K} = \mathbf{F} \circ \mathbf{B} \quad , \quad \mathbf{S}_\infty = (\mathbf{I} - \mathbf{K})^{-1} \mathbf{F} \quad (9)$$

where \circ is the Hadamard product and \mathbf{K} combines first interaction probabilities with single reflection-scattering probabilities, and \mathbf{S}_∞ describes reflection-scattering paths. The absorption matrix \mathbf{A} and the multiple reflection-scattering matrix \mathbf{R} are expressed as:

$$\mathbf{A} = (\mathbf{1} - \mathbf{B})^T \circ \mathbf{S}_\infty \circ (\mathbf{1} - \mathbf{B}) \quad (10)$$

$$\mathbf{R} = (\mathbf{1} - \mathbf{B})^T \circ \mathbf{S}_\infty \circ \mathbf{B} \quad (11)$$

where $\mathbf{1}$ is a matrix of ones. The first matrix, $(\mathbf{1} - \mathbf{B})^T$, accounts for the probability of emission, the middle matrix, \mathbf{S}_∞ , accounts for all possible reflection-scattering paths at the steady-state, and the last matrices, $\mathbf{1} - \mathbf{B}$ or \mathbf{B} account for absorption or reflection at the destination.

2.3. Application of the Transformed Exchange Factors

Next, based on fundamental radiative energy balances, which state that an energy source is equal to the total radiant power, minus the absorbed power, minus the reflected incident power, and that the emissive power equals the total radiant power, minus the reflected incident power, the matrices \mathbf{C} and \mathbf{D} are defined as:

$$\mathbf{C} = \mathbf{I} - \mathbf{A}^T - \mathbf{R}^T \quad , \quad \mathbf{D} = \mathbf{I} - \mathbf{R}^T \quad (12)$$

Now, given a vector \mathbf{e} of the emissive powers and a vector \mathbf{q} of the source terms of each element, where only one entry of these can be specified for each element, the mixed-boundary matrix \mathbf{M} can be assembled row by row:

$$\mathbf{M}[i, :] = \mathbf{C}[i, :] \quad , \quad \mathbf{M}[j, :] = \mathbf{D}[j, :] \quad (13)$$

using i for known entries of the source vector \mathbf{q}_i and using j for known entries of the emissive power vector \mathbf{e}_j , where i and j are mutually exclusive. Next, the linear system:

$$\mathbf{M}\mathbf{j} = \mathbf{h} \quad (14)$$

is solved for the total radiant power \mathbf{j} of each element, where \mathbf{h} is a vector of known emissive powers or source terms, depending on which is known, corresponding to the i and j rows of \mathbf{M} .

Knowing the total radiant power of each element, the absorbed incident power \mathbf{g}_a and the unknown terms of the emissive power vector \mathbf{e} and the source term vector \mathbf{q} can be determined from:

$$\mathbf{g}_a = \mathbf{A}^T \mathbf{j} \quad , \quad \mathbf{e}_i = \mathbf{q}_i + \mathbf{g}_{a,i} \quad , \quad \mathbf{q}_j = \mathbf{e}_j - \mathbf{g}_{a,j} \quad (15)$$

where i and j are again mutually exclusive. The reflected-scattered power \mathbf{r} and the total incident power \mathbf{g} can be determined from:

$$\mathbf{r} = \mathbf{R}^T \mathbf{j} \quad , \quad \mathbf{g} = \mathbf{g}_a + \mathbf{r} \quad (16)$$

The total intensity of volumes and of Lambertian surfaces can be determined from:

$$\mathbf{i}_{V,i} = \frac{\mathbf{j}_{V,i}}{4\pi V_i} \quad , \quad \mathbf{i}_{S,i} = \frac{\mathbf{j}_{S,i}}{\pi A_i} \quad (17)$$

Finally the temperature of each element can be determined from its emissive power using ε and κ and the Stefan-Boltzmann law:

$$T_{s,i} = \left(\frac{\mathbf{e}_{s,i}}{\varepsilon_{s,i} \sigma A_{s,i}} \right)^{1/4} \quad , \quad T_{g,i} = \left(\frac{\mathbf{e}_{g,i}}{4\kappa_i \sigma V_{g,i} n_i^2} \right)^{1/4} \quad (18)$$

where σ is the Stefan-Boltzmann constant and n_i is the refractive index of the medium of element i .

As mentioned in the introduction, for a medium with varying refractive index, \mathbf{F} should be obtained by solving differential equations for each ray trajectory. While differential equations require a continuously changing refractive index, the proposed transformation uses a discrete mesh of the domain. For this reason, a mean value of the refractive index in each volume element should be used in equation (18) to calculate the temperature. The ray trajectories in a medium with variable refractive index are found by solving the following vector differential equation for each ray [14]:

$$\frac{d}{dS} \left(n \frac{d\mathbf{x}}{dS} \right) = \nabla n \quad (19)$$

where \mathbf{x} is the position and S is the distance along a ray path and ∇ is the gradient operator. Since the proposed method uses only the points of emission and first interaction, everything regarding the geometric ray trajectories is handled during the ray tracing step. This distinction is natural: the continuous differential equation governs ray propagation physics, while the discrete exchange factors capture the resulting energy transfer between finite elements.

3. Convergence Properties

This section presents the essential convergence guarantees of the proposed transformation through two fundamental theorems which characterize the steady state path matrix.

Theorem 3.1 (Convergence and Irreducibility of the Steady State Path). *Let \mathbf{F} be the row stochastic irreducible exchange factor matrix, let \mathbf{B} be the column constant single reflection-scattering matrix and let $\mathbf{K} = \mathbf{F} \circ \mathbf{B}$ be the single reflection-scattering interaction matrix. The steady state path matrix is defined as:*

$$\mathbf{S}_\infty = \lim_{N \rightarrow \infty} \sum_{i=0}^N \mathbf{K}^i \mathbf{F} = (\mathbf{I} - \mathbf{K})^{-1} \mathbf{F} \quad (20)$$

Then \mathbf{S}_∞ exists, is finite and irreducible if and only if the spectral radius $\rho(\mathbf{K}) < 1$. Moreover, the spectral radius satisfies:

$$0 \leq \min_j(\mathbf{B}) \leq \min_i \sum_j \mathbf{K} \leq \rho(\mathbf{K}) \leq \max_i \sum_j \mathbf{K} \leq \max_j(\mathbf{B}) < 1 \quad (21)$$

Proof. Each entry of \mathbf{F} represents the probability of a ray travelling from emitter i to interact with element j . The accumulated probability after N reflections or scatterings is given by the finite sum:

$$\mathbf{S}_N = \mathbf{F} + \mathbf{K}\mathbf{F} + \mathbf{K}^2\mathbf{F} + \cdots + \mathbf{K}^N\mathbf{F} = \left(\sum_{i=0}^N \mathbf{K}^i \right) \mathbf{F} \quad (22)$$

By the Neumann series theorem, $\sum_{i=0}^{\infty} \mathbf{K}^i = (\mathbf{I} - \mathbf{K})^{-1}$ converges if and only if $\rho(\mathbf{K}) < 1$ [18].

The bounds on $\rho(\mathbf{K})$ follow from Gershgorin's disk theorem applied to the non-negative matrix \mathbf{K} , where \mathbf{B} represents the column constant matrix of reflection-scattering coefficients.

Since the infinite series for the inverse $(\mathbf{I} - \mathbf{K})^{-1}$ always contains the identity matrix, $(\mathbf{I} - \mathbf{K})^{-1}\mathbf{F}$ always contains \mathbf{F} , and since remaining terms in the series are non-negative, the connectivity in the domain can only increase with $\mathbf{B} > \mathbf{0}$, hence the irreducibility of \mathbf{F} is preserved in \mathbf{S}_{∞} . ■

Remark 3.2. The physical interpretation ensures convergence: as long as at least a single element with reflection-scattering coefficient strictly less than unity is visible from all elements, infinite reflection-scattering paths are prevented.

Theorem 3.3 (Numerical Stability of the Steady State Path). *Let $\mathbf{I} - \mathbf{K}$ be the matrix to be inverted in the calculation of the steady state path matrix. Then the determinant of $\mathbf{I} - \mathbf{K}$ satisfies:*

$$\prod_{i=1}^{m+n} \left(1 - \sum_j \mathbf{K}_{ij} \right) \leq \det(\mathbf{I} - \mathbf{K}) \leq \prod_{i=1}^{m+n} \left(1 - \mathbf{K}_{ii} + \sum_{j \neq i} \mathbf{K}_{ij} \right) \quad (23)$$

where $m + n$ is the matrix dimension. For uniform reflection-scattering coefficient γ , numerical feasibility requires:

$$\epsilon \leq (1 - \gamma)^{m+n} \implies \gamma \leq 1 - \epsilon^{1/(m+n)} \implies m + n \leq \left\lfloor \frac{\ln(\epsilon)}{\ln(1 - \gamma)} \right\rfloor \quad (24)$$

where ϵ is the machine precision and $\lfloor \cdot \rfloor$ is the floor function.

Proof. Gershgorin's disk theorem is applied to $\mathbf{I} - \mathbf{K}$. The diagonal and off-diagonal elements are:

$$(\mathbf{I} - \mathbf{K})_{ii} = 1 - \mathbf{K}_{ii}, \quad (\mathbf{I} - \mathbf{K})_{i \neq j} = -\mathbf{K}_{i \neq j} \quad (25)$$

Each eigenvalue λ_i lies within at least one Gershgorin disk [18]:

$$|\lambda_i - (1 - \mathbf{K}_{ii})| \leq \sum_{j \neq i} \mathbf{K}_{ij} \quad (26)$$

Disk i is centered at $1 - \mathbf{K}_{ii}$ with radius $\sum_{j \neq i} \mathbf{K}_{ij}$, giving leftmost point at $1 - \sum_j \mathbf{K}_{ij}$ and rightmost at $1 - \mathbf{K}_{ii} + \sum_{j \neq i} \mathbf{K}_{ij}$.

Since $\det(\mathbf{I} - \mathbf{K}) = \prod_i \lambda_i$, the bounds follow from taking the product over extreme eigenvalue positions.

For uniform γ and row-stochastic \mathbf{F} , the lower bound becomes $(1 - \gamma)^{m+n}$. Requiring that this exceeds machine precision ϵ gives the numerical feasibility conditions. ■

4. Matrix Properties

This section will explore the properties of the matrices of the proposed exchange factor transformation. These properties will subsequently be used to establish conditions which guarantee physical correctness.

4.1. Spectral Radii of the Absorption and Reflection-Scattering Matrices

This section determines bounds on the spectral radii of \mathbf{A} and \mathbf{R} .

Theorem 4.1 (Spectral Radius of Combined Absorption and Reflection-Scattering). *Let \mathbf{F} be the row stochastic and irreducible exchange factor matrix, and let \mathbf{A} and \mathbf{R} be the absorption and multiple reflection-scattering matrices defined by the exchange factor transformation, and let \mathbf{P} be the diagonal matrix with entries $\mathbf{P}_{ii} = 1 - \mathbf{b}_i$ where \mathbf{b}_i are the reflection-scattering coefficients. Then:*

1. The sum $\mathbf{A} + \mathbf{R}$ can be expressed as

$$\mathbf{A} + \mathbf{R} = \mathbf{P}(\mathbf{I} - \mathbf{K})^{-1}\mathbf{F} \quad (27)$$

2. The spectral radius satisfies $\rho(\mathbf{A} + \mathbf{R}) = 1$
3. The vector $\mathbf{v} = (\mathbf{1} - \mathbf{b})$ is the Perron eigenvector corresponding to the positive real eigenvalue $\lambda = 1$

Proof. The result is established through a sequence of key relationships.

Step 1: The fundamental vector relationship is established:

$$[\mathbf{F}(\mathbf{1} - \mathbf{b})]_i = \sum_j \mathbf{F}_{ij}(1 - \mathbf{b}_j) = \sum_j \mathbf{F}_{ij} - \sum_j \mathbf{F}_{ij}\mathbf{b}_j = 1 - \sum_j \mathbf{K}_{ij} \quad (28)$$

Step 2: The corresponding property for $(\mathbf{I} - \mathbf{K})$ is established:

$$[(\mathbf{I} - \mathbf{K})\mathbf{1}]_i = \sum_j (\delta_{ij} - \mathbf{K}_{ij}) = 1 - \sum_j \mathbf{K}_{ij} \quad (29)$$

Step 3: Steps 1 and 2 are combined to obtain the key identity:

$$\mathbf{F}(\mathbf{1} - \mathbf{b}) = (\mathbf{I} - \mathbf{K})\mathbf{1} \quad (30)$$

Step 4: Left-multiplying equation (30) by the inverse $(\mathbf{I} - \mathbf{K})^{-1}$:

$$(\mathbf{I} - \mathbf{K})^{-1}\mathbf{F}(\mathbf{1} - \mathbf{b}) = \mathbf{1} \quad (31)$$

Step 5: Left-multiplying by the diagonal matrix \mathbf{P} yields:

$$\mathbf{P}(\mathbf{I} - \mathbf{K})^{-1}\mathbf{F}(\mathbf{1} - \mathbf{b}) = \mathbf{P}\mathbf{1} \quad (32)$$

Step 6: Recognizing part of the left-hand side of equation (32) as $\mathbf{A} + \mathbf{R}$:

$$\mathbf{A} + \mathbf{R} = (\mathbf{1} - \mathbf{B})^T \circ \mathbf{S}_\infty \circ (\mathbf{1} - \mathbf{B}) + (\mathbf{1} - \mathbf{B})^T \circ \mathbf{S}_\infty \circ \mathbf{B} \quad (33)$$

$$= (\mathbf{1} - \mathbf{B})^T \circ \mathbf{S}_\infty \quad (34)$$

$$= \mathbf{P}(\mathbf{I} - \mathbf{K})^{-1}\mathbf{F} \quad (35)$$

Step 7: Combining with $\mathbf{P}\mathbf{1} = \mathbf{1} - \mathbf{b}$ yields the final eigenvalue identity:

$$(\mathbf{A} + \mathbf{R})(\mathbf{1} - \mathbf{b}) = \mathbf{1} - \mathbf{b} \quad (36)$$

Therefore, $\mathbf{v} = \mathbf{1} - \mathbf{b}$ is an eigenvector with real eigenvalue $\lambda = 1$. Since all components of \mathbf{v} are positive (assuming $\mathbf{b}_i < 1$ for convergence), this is the Perron eigenvector. By the Perron-Frobenius theorem, the corresponding eigenvalue equals the spectral radius [18], hence $\rho(\mathbf{A} + \mathbf{R}) = 1$. ■

Theorem 4.2 (Spectral Radius of Absorption). *Let \mathbf{A} be the absorption matrix of the exchange factor transformation and \mathbf{P} be the diagonal matrix with entries $\mathbf{P}_{ii} = 1 - \mathbf{b}_i$. Then:*

1. *The absorption matrix can be expressed as:*

$$\mathbf{A} = (\mathbf{A} + \mathbf{R})\mathbf{P} \quad (37)$$

2. *The row sums of \mathbf{A} satisfy:*

$$[\mathbf{A}\mathbf{1}]_i = 1 - \mathbf{b}_i \quad (38)$$

3. *The spectral radius is bounded by:*

$$1 - \max_i \mathbf{b}_i \leq \rho(\mathbf{A}) \leq 1 - \min_i \mathbf{b}_i \quad (39)$$

In the limiting case $\mathbf{b}_i = 0$, this recovers the row-stochastic spectral radius of unity for \mathbf{F} .

Proof. **Step 1:** The matrix decomposition is established. From equations (10) and (11):

$$\mathbf{A} + \mathbf{R} = (\mathbf{1} - \mathbf{B})^T \circ \mathbf{S}_\infty \circ (\mathbf{1} - \mathbf{B}) + (\mathbf{1} - \mathbf{B})^T \circ \mathbf{S}_\infty \circ \mathbf{B} \quad (40)$$

$$= (\mathbf{1} - \mathbf{B})^T \circ \mathbf{S}_\infty \quad (41)$$

From the definition of \mathbf{A} in equation (10) this leads to

$$\mathbf{A} = (\mathbf{A} + \mathbf{R}) \circ (\mathbf{1} - \mathbf{B}) \quad (42)$$

Since \mathbf{B} is column constant, the Hadamard product of equation (42) is equivalent to right matrix multiplication by the diagonal matrix \mathbf{P} :

$$\mathbf{A} = (\mathbf{A} + \mathbf{R})\mathbf{P} \quad (43)$$

Step 2: The row sums are computed using the eigenvalue relationship. From Theorem 4.1, it is known that $(\mathbf{A} + \mathbf{R})(\mathbf{1} - \mathbf{b}) = \mathbf{1} - \mathbf{b}$. Therefore:

$$[\mathbf{A}\mathbf{1}]_i = [(\mathbf{A} + \mathbf{R})\mathbf{P}\mathbf{1}]_i \quad (44)$$

$$= [(\mathbf{A} + \mathbf{R})(\mathbf{1} - \mathbf{b})]_i \quad (45)$$

$$= 1 - \mathbf{b}_i \quad (46)$$

Step 3: The spectral radius bounds are derived. Since $[\mathbf{A}\mathbf{1}]_i = 1 - \mathbf{b}_i$, the row sums range from $1 - \max_i \mathbf{b}_i$ to $1 - \min_i \mathbf{b}_i$. By the Gershgorin disk theorem and properties of non-negative matrices, the spectral radius satisfies [18]:

$$1 - \max_i \mathbf{b}_i \leq \rho(\mathbf{A}) \leq 1 - \min_i \mathbf{b}_i \quad (47)$$

When $\mathbf{b}_i = 0$ for all i , the exchange factor transformation yields $\mathbf{A} = \mathbf{F}$, and the bounds collapse to $\rho(\mathbf{A}) = 1$, consistent with the row-stochastic property of the exchange factor matrix. \blacksquare

Theorem 4.3 (Upper Bound on Spectral Radius of Reflection-Scattering). *The spectral radius of the multiple reflection-scattering matrix \mathbf{R} of the exchange factor transformation satisfies:*

$$\rho(\mathbf{R}) \leq (1 - \min_i \mathbf{b}_i) \frac{\|\mathbf{K}\|_\infty}{1 - \|\mathbf{K}\|_\infty} \quad (48)$$

For physical realizability, the bound on $\rho(\mathbf{R})$ must be less than unity, requiring:

$$\|\mathbf{K}\|_\infty < \frac{1}{2 - \min_i \mathbf{b}_i} \quad (49)$$

Proof. From the eigenvalue equation $(\mathbf{A} + \mathbf{R})(\mathbf{1} - \mathbf{b}) = \mathbf{1} - \mathbf{b}$ and using $\mathbf{A}\mathbf{1} = \mathbf{1} - \mathbf{b}$:

$$(\mathbf{A} + \mathbf{R})(\mathbf{1} - \mathbf{b}) = \mathbf{1} - \mathbf{b} \quad (50)$$

$$\mathbf{A}\mathbf{1} + \mathbf{R}\mathbf{1} - \mathbf{Ab} - \mathbf{Rb} = \mathbf{1} - \mathbf{b} \quad (51)$$

$$\mathbf{R}\mathbf{1} - \mathbf{Ab} - \mathbf{Rb} = \mathbf{0} \quad (52)$$

$$\mathbf{R}\mathbf{1} = (\mathbf{A} + \mathbf{R})\mathbf{b} \quad (53)$$

Substituting $\mathbf{A} + \mathbf{R} = \mathbf{P}(\mathbf{I} - \mathbf{K})^{-1}\mathbf{F}$ and applying submultiplicativity:

$$\mathbf{R}\mathbf{1} = \mathbf{P}(\mathbf{I} - \mathbf{K})^{-1}\mathbf{F}\mathbf{b} \quad (54)$$

$$\|\mathbf{R}\|_{\infty} \leq \|\mathbf{P}\|_{\infty} \|(\mathbf{I} - \mathbf{K})^{-1}\|_{\infty} \|\mathbf{K}\|_{\infty} \quad (55)$$

$$\leq \max_i (1 - \mathbf{b}_i) \frac{1}{1 - \|\mathbf{K}\|_{\infty}} \|\mathbf{K}\|_{\infty} \quad (56)$$

Since $\rho(\mathbf{R}) \leq \|\mathbf{R}\|_{\infty}$, the bound follows. The physical constraint comes from requiring that $\mathbf{D} = \mathbf{I} - \mathbf{R}^T$ is invertible, which is necessary for \mathbf{M} of equation (14) to be invertible. By the Neumann series theorem, the inverse $\mathbf{D}^{-1} = (\mathbf{I} - \mathbf{R}^T)^{-1}$ exists when $\rho(\mathbf{R}) < 1$ [18]. \blacksquare

Theorem 4.4 (Spectral Radius of Reflection-Scattering for Uniform Properties). *When the reflection-scattering coefficients are uniform, $\mathbf{b}_i = \gamma$ for all i where $\gamma \in [0, 1]$, then:*

1. The vector $\mathbf{b} = \gamma\mathbf{1}$ is an eigenvector of \mathbf{R} with eigenvalue γ
2. The spectral radius satisfies $\rho(\mathbf{R}) = \gamma$

Proof. For uniform γ , we have $\mathbf{P} = (1 - \gamma)\mathbf{I}$ and $\mathbf{K} = \gamma\mathbf{F}$.

Step 1: The key relationship is developed:

$$(\mathbf{I} - \mathbf{K})\mathbf{b} = \gamma\mathbf{1} - \gamma\mathbf{F}\mathbf{b} = \gamma\mathbf{1} - \gamma^2\mathbf{F}\mathbf{1} = \gamma(1 - \gamma)\mathbf{1} = (1 - \gamma)\mathbf{b} \quad (57)$$

Step 2: The eigenvalue property is established. From Step 1: $(\mathbf{I} - \mathbf{K})^{-1}\mathbf{b} = \frac{\mathbf{b}}{1 - \gamma}$
Computing $\mathbf{R}\mathbf{b}$:

$$(\mathbf{A} + \mathbf{R})\mathbf{b} = \mathbf{P}(\mathbf{I} - \mathbf{K})^{-1}\mathbf{F}\mathbf{b} \quad (58)$$

$$= (1 - \gamma) \frac{\gamma}{1 - \gamma} \mathbf{1} = \gamma\mathbf{1} = \mathbf{b} \quad (59)$$

Since $\mathbf{Ab} = \gamma\mathbf{A}\mathbf{1} = \gamma(1 - \gamma)\mathbf{1}$:

$$\mathbf{R}\mathbf{b} = (\mathbf{A} + \mathbf{R})\mathbf{b} - \mathbf{Ab} = \gamma\mathbf{1} - \gamma(1 - \gamma)\mathbf{1} = \gamma^2\mathbf{1} = \gamma\mathbf{b} \quad (60)$$

This shows that $\mathbf{b} = \gamma\mathbf{1}$ is an eigenvector of \mathbf{R} with eigenvalue γ .

Step 3: The spectral radius is established. From Theorem 4.3, the upper bound is:

$$\rho(\mathbf{R}) \leq (1 - \min_i \mathbf{b}_i) \frac{\|\mathbf{K}\|_{\infty}}{1 - \|\mathbf{K}\|_{\infty}} \quad (61)$$

For uniform γ : $\min_i \mathbf{b}_i = \gamma$. Since $\mathbf{K} = \gamma\mathbf{F}$ and \mathbf{F} is row-stochastic, $\|\mathbf{K}\|_{\infty} = \gamma$. Substituting:

$$\rho(\mathbf{R}) \leq (1 - \gamma) \frac{\gamma}{1 - \gamma} = \gamma \quad (62)$$

Since γ is an eigenvalue (from Step 2), $\rho(\mathbf{R}) \geq \gamma$. Combined with the upper bound, $\rho(\mathbf{R}) = \gamma$. \blacksquare

Theorem 4.5 (Spectral Radius Sum Property). *For uniform reflection-scattering coefficients $\mathbf{b}_i = \gamma$, the spectral radii of the absorption and multiple reflection-scattering matrices satisfy:*

$$\rho(\mathbf{A}) + \rho(\mathbf{R}) = \rho(\mathbf{A} + \mathbf{R}) = 1 \quad (63)$$

For uniform reflection-scattering coefficients, the Perron eigenvalues of \mathbf{A} , \mathbf{R} , and $\mathbf{A} + \mathbf{R}$ are real.

Proof. From Theorems 4.2 and 4.4:

- $\rho(\mathbf{A}) = 1 - \gamma$ (uniform case)
- $\rho(\mathbf{R}) = \gamma$ (uniform case)
- $\rho(\mathbf{A} + \mathbf{R}) = 1$

Therefore: $\rho(\mathbf{A}) + \rho(\mathbf{R}) = (1 - \gamma) + \gamma = 1 = \rho(\mathbf{A} + \mathbf{R})$. Since $\gamma = \mathbf{b}_i$ is real, all Perron eigenvalues are real. \blacksquare

4.2. Non-negativity of the Inverse of the Mixed Boundary Matrix

To ensure non-negative radiation for the proposed transformation, the inverse of the mixed boundary matrix \mathbf{M} of equation (14) should be non-negative. This requires establishing that both component matrices \mathbf{C} and \mathbf{D} are M-matrices and that \mathbf{M} is non-singular.

Theorem 4.6 (M-matrix Property of \mathbf{C}). *The matrix $\mathbf{C} = \mathbf{I} - \mathbf{A}^T - \mathbf{R}^T$ is a singular M-matrix with the following properties:*

1. \mathbf{C} has zero as the eigenvalue with the smallest real part, with left eigenvector $(\mathbf{1} - \mathbf{b})^T$
2. The diagonal entries satisfy $\mathbf{C}_{ii} \geq 0$ for all i
3. The off-diagonal entries satisfy $\mathbf{C}_{ij} \leq 0$ for all $i \neq j$

Proof. Step 1: The zero eigenvalue is established as the smallest real part eigenvalue. From the row sum properties established in previous theorems:

$$\mathbf{A}\mathbf{1} + \mathbf{R}\mathbf{1} = (\mathbf{1} - \mathbf{b}) + (\mathbf{A} + \mathbf{R})\mathbf{b} \quad (64)$$

$$(\mathbf{I} - \mathbf{A} - \mathbf{R})\mathbf{b} = (\mathbf{I} - \mathbf{A} - \mathbf{R})\mathbf{1} \quad (65)$$

$$\mathbf{C}^T(\mathbf{1} - \mathbf{b}) = \mathbf{0} \quad (66)$$

Therefore, $(\mathbf{1} - \mathbf{b})^T$ is a left eigenvector of \mathbf{C} with eigenvalue zero. Since $\mathbf{C} = \mathbf{I} - \mathbf{A}^T - \mathbf{R}^T$, if λ is an eigenvalue of $\mathbf{A} + \mathbf{R}$, then $1 - \lambda$ is an eigenvalue of \mathbf{C} . From theorem 4.1, $\mathbf{1} - \mathbf{b}$ corresponds to the Perron eigenvector of $\mathbf{A} + \mathbf{R}$ with spectral radius of unity. This shows that zero is the smallest real part of any eigenvalue of \mathbf{C} .

Step 2: The non-negative diagonal entries are established. From the eigenvalue equation $\mathbf{C}^T(\mathbf{1} - \mathbf{b}) = \mathbf{0}$:

$$0 = [\mathbf{C}^T(\mathbf{1} - \mathbf{b})]_i \quad (67)$$

$$= (1 - (\mathbf{A} + \mathbf{R})_{ii})(1 - \mathbf{b}_i) - \sum_{j \neq i} (\mathbf{A} + \mathbf{R})_{ij}(1 - \mathbf{b}_j) \quad (68)$$

Solving for the diagonal:

$$\mathbf{C}_{ii} = 1 - (\mathbf{A} + \mathbf{R})_{ii} = \sum_{j \neq i} (\mathbf{A} + \mathbf{R})_{ij} \frac{1 - \mathbf{b}_j}{1 - \mathbf{b}_i} \geq 0 \quad (69)$$

since all terms are non-negative.

Step 3: Off-diagonal entries are non-positive by construction since $\mathbf{C}_{ij} = -(\mathbf{A}^T + \mathbf{R}^T)_{ij} \leq 0$ for $i \neq j$. \blacksquare

Theorem 4.7 (M-matrix Property of \mathbf{D}). *The matrix $\mathbf{D} = \mathbf{I} - \mathbf{R}^T$ is a non-singular M-matrix with the following properties:*

1. All eigenvalues have real parts bounded below: $\text{Re}(\lambda_{\mathbf{D}}) \geq 1 - \rho(\mathbf{R})$
2. The diagonal entries satisfy $\mathbf{D}_{ii} \geq 0$ for all i
3. The off-diagonal entries satisfy $\mathbf{D}_{ij} \leq 0$ for all $i \neq j$

As long as $\rho(\mathbf{R}) < 1$, \mathbf{D} is guaranteed to be non-singular.

Proof. **Step 1:** Eigenvalue bounds. Since $\mathbf{D} = \mathbf{I} - \mathbf{R}^T$, if λ is an eigenvalue of \mathbf{R} , then $1 - \lambda$ is an eigenvalue of \mathbf{D} . From Theorem 4.3:

$$\text{Re}(\lambda_{\mathbf{D}}) \geq 1 - \rho(\mathbf{R}) \geq 1 - (1 - \min_i \mathbf{b}_i) \frac{\|\mathbf{K}\|_{\infty}}{1 - \|\mathbf{K}\|_{\infty}} \quad (70)$$

Step 2: Non-negative diagonal entries. Since $\mathbf{D} = \mathbf{C} + \mathbf{A}^T$ and both \mathbf{C} (from Theorem 4.6) and \mathbf{A}^T have non-negative diagonal entries:

$$\mathbf{D}_{ii} = \mathbf{C}_{ii} + \mathbf{A}_{ii} \geq 0 \quad (71)$$

Step 3: Off-diagonal entries are non-positive by construction since $\mathbf{D}_{ij} = -\mathbf{R}_{ij}^T \leq 0$ for $i \neq j$. \blacksquare

Theorem 4.8 (Non-singularity of Mixed Boundaries). *Let $\mathbf{A}, \mathbf{R}, \mathbf{C}, \mathbf{D}$ be the system matrices defined by the proposed exchange factor transform, let \mathbf{F} be the irreducible and row stochastic exchange factor matrix, and let $\mathbf{1} - \mathbf{b}$ be the Perron eigenvector of $\mathbf{A} + \mathbf{R}$. Then any matrix \mathbf{M} obtained by replacing at least one row of \mathbf{C} with the corresponding row from \mathbf{D} is non-singular.*

Proof. **Step 1:** Application of established spectral properties. By Theorem 4.1, $\mathbf{A} + \mathbf{R}$ has spectral radius $\rho(\mathbf{A} + \mathbf{R}) = 1$ with corresponding Perron eigenvector $\mathbf{1} - \mathbf{b} > \mathbf{0}$. Since \mathbf{F} and \mathbf{S}_{∞} are both irreducible and the positive diagonal $\mathbf{P}_{ii} = 1 - \mathbf{b}_i > 0$ cannot change connectivity, the matrix $\mathbf{A} + \mathbf{R} = \mathbf{P}\mathbf{S}_{\infty}$ is irreducible. By the Perron-Frobenius theorem, eigenvalue 1 has geometric multiplicity exactly 1 [18].

Step 2: Positive column sums of \mathbf{A} . Since \mathbf{F} is irreducible, every column j has at least one positive entry (otherwise element j would be unreachable). The infinite series form of $\mathbf{S}_{\infty} = (\sum_{i=0}^N \mathbf{K}^i) \mathbf{F}$ shows that the matrix \mathbf{S}_{∞} inherits the property that each column has positive sum.

Therefore, \mathbf{A} , which can be formulated as $\mathbf{A} = \mathbf{P}\mathbf{S}_{\infty}\mathbf{P}$ with positive diagonal \mathbf{P} , preserves this structure, ensuring that each column of \mathbf{A} has at least one positive entry.

Step 3: Non-singularity of \mathbf{M} . By Theorem 4.6, \mathbf{C}^T has nullity (dimension of null space) exactly 1 with $\text{null}(\mathbf{C}^T) = \text{span}\{\mathbf{1} - \mathbf{b}\}$. Since $\text{nullity}(\mathbf{C}) = \text{nullity}(\mathbf{C}^T) = 1$, it is obtained that $\text{rank}(\mathbf{C}) = n - 1$.

Let \mathbf{M} be obtained by replacing at least one row of \mathbf{C} with the corresponding row from \mathbf{D} . Without loss of generality, assume the j -th row is replaced. Then, since $\mathbf{D} = \mathbf{C} + \mathbf{A}^T$:

$$\mathbf{M} = \mathbf{C} + \mathbf{e}_j(\mathbf{A}^T)_j \quad (72)$$

where $(\mathbf{A}^T)_j$ denotes the j -th row of \mathbf{A}^T and \mathbf{e}_j is the j -th standard basis vector.

Since $(\mathbf{1} - \mathbf{b})^T \mathbf{C} = \mathbf{0}$, it is obtained that:

$$(\mathbf{1} - \mathbf{b})^T \mathbf{M} = (\mathbf{1} - \mathbf{b})^T \mathbf{C} + (\mathbf{1} - \mathbf{b})^T (\mathbf{e}_j (\mathbf{A}^T)_j) = (1 - b_j) (\mathbf{A}^T)_j \quad (73)$$

Since $\mathbf{A} \geq \mathbf{0}$, $(1 - b_j) > 0$, and step 2 ensures \mathbf{A} has at least one positive entry in each column, it is obtained that $(\mathbf{1} - \mathbf{b})^T \mathbf{M} \neq \mathbf{0}$.

Therefore $(\mathbf{1} - \mathbf{b}) \notin \text{null}(\mathbf{M}^T)$, which means $\text{nullity}(\mathbf{M}^T) < \text{nullity}(\mathbf{C}^T) = 1$.

Since $\text{nullity}(\mathbf{M}^T) = \text{nullity}(\mathbf{M})$, it is obtained that $\text{nullity}(\mathbf{M}) = 0$, so \mathbf{M} is non-singular. ■

Remark 4.9. The irreducibility of the exchange factor matrix \mathbf{F} is crucial for this result. In radiative transfer applications, \mathbf{F} represents connectivity within a physical domain. The matrix \mathbf{F} is irreducible if and only if the underlying domain has no isolated regions, that is, for any two regions i and j , there exists a sequence of direct sight lines connecting them. This physical connectivity condition naturally ensures the mathematical irreducibility required for the theorem.

5. Physical Correctness

For a physical model to be useful it should possess physical correctness. The conditions which guarantee physical correctness of results calculated with the proposed exchange factor transformation are described in the following subsections.

5.1. Non-Negative Radiation

For radiative transfer, physical correctness means that the calculated rate of radiation must be non-negative, since negative radiation is not a physically meaningful quantity.

Theorem 5.1 (Non-negative Radiation). *Under the conditions established in the previous theorems, the exchange factor transformation guarantees physical correctness through non-negative radiation quantities:*

1. Non-negative total radiant power: $\mathbf{j} = \mathbf{M}^{-1} \mathbf{h} \geq \mathbf{0}$ for non-negative source terms $\mathbf{h} \geq \mathbf{0}$
2. Non-negative reflected-scattered power: $\mathbf{r} = \mathbf{R}^T \mathbf{j} \geq \mathbf{0}$
3. Non-negative emissive power: $\mathbf{e} = (\mathbf{I} - \mathbf{R}^T) \mathbf{j} = \mathbf{q} + \mathbf{A}^T \mathbf{j} \geq \mathbf{0}$

Proof. Part 1: Non-negative total radiant power. From Theorems 4.6, 4.7 and 4.8, the mixed boundary matrix \mathbf{M} is a non-singular M-matrix. By the fundamental property of M-matrices, $\mathbf{M}^{-1} \geq \mathbf{0}$. Therefore, for non-negative source terms $\mathbf{h} \geq \mathbf{0}$:

$$\mathbf{j} = \mathbf{M}^{-1} \mathbf{h} \geq \mathbf{0} \quad (74)$$

Part 2: Non-negative reflected-scattered power. Since $\mathbf{R} \geq \mathbf{0}$ by construction and $\mathbf{j} \geq \mathbf{0}$ from Part 1:

$$\mathbf{r} = \mathbf{R}^T \mathbf{j} \geq \mathbf{0} \quad (75)$$

Part 3: Non-negative emissive power. The emissive power can be expressed in two equivalent forms due to internal consistency of the proposed exchange factor transformation:

$$\mathbf{e} = (\mathbf{I} - \mathbf{R}^T) \mathbf{j} = \mathbf{q} + \mathbf{A}^T \mathbf{j} \quad (76)$$

Since $\mathbf{A} \geq \mathbf{0}$ by construction, $\mathbf{j} \geq \mathbf{0}$ from Part 1, and assuming non-negative prescribed source terms $\mathbf{q} \geq \mathbf{0}$:

$$\mathbf{e} = \mathbf{q} + \mathbf{A}^T \mathbf{j} \geq \mathbf{0} \quad (77)$$

The equivalence in equation (76) reveals that the entries of \mathbf{j} perfectly balance the entries of $\mathbf{I} - \mathbf{R}^T$, ensuring physical consistency. ■

5.2. Conservation of Energy

At the steady state, energy conservation requires that the source fluxes $\mathbf{q} = \mathbf{Cj}$ calculated from any total radiant power solution vector \mathbf{j} sum to a scalar of zero: $\mathbf{1}^T \mathbf{Cj} = 0$. This fundamental physical principle places constraints on the reflection-scattering coefficients and boundary conditions of the proposed exchange factor transformation.

Theorem 5.2 (Energy Conservation - Uniform Reflection-Scattering Coefficients). *Let \mathbf{F} be the row-stochastic exchange factor matrix, and let $\mathbf{b} = \gamma \mathbf{1}$ be the uniform vector of coefficients for the column constant single reflection-scattering matrix \mathbf{B} for some scalar $\gamma \in [0, 1]$, and define the remaining system matrices as given by the proposed exchange factor transformation.*

Then for any mixed system $\mathbf{Mj} = \mathbf{h}$ where \mathbf{M} is assembled from rows of \mathbf{C} and \mathbf{D} , the sum of the source fluxes equal zero, meaning the energy conservation property holds:

$$\mathbf{1}^T \mathbf{Cj} = 0 \quad (78)$$

regardless of the choice of rows or non-negative boundary conditions in the mixed system.

Proof. For uniform $\mathbf{b} = \gamma \mathbf{1}$, the eigenvalue condition $(\mathbf{1} - \mathbf{b})^T \mathbf{C} = \mathbf{0}^T$ of Theorem 4.6 becomes:

$$(\mathbf{1} - \gamma \mathbf{1})^T \mathbf{C} = (1 - \gamma) \mathbf{1}^T \mathbf{C} = \mathbf{0}^T \quad (79)$$

Since $1 - \gamma > 0$, the following property is obtained: $\mathbf{1}^T \mathbf{C} = \mathbf{0}^T$. Therefore: $\mathbf{1}^T \mathbf{Cj} = \mathbf{0}^T \mathbf{j} = 0$ for any vector \mathbf{j} . This establishes energy conservation automatically, regardless of how the mixed system is constructed. \blacksquare

Theorem 5.3 (Energy Conservation - Non-Uniform Reflection-Scattering Coefficients). *Let \mathbf{F} be row stochastic, $0 \leq \mathbf{B}_j < 1$ be column constant, and define the system matrices as given by the proposed exchange factor transformation. Consider a mixed system $\mathbf{Mj} = \mathbf{h}$ where:*

- Rows I of \mathbf{M} are taken from \mathbf{C} with corresponding uniform $\mathbf{h}_I = \mathbf{0}$
- \mathbf{B} can be non-uniform on rows I : $0 \leq \mathbf{B}_i < 1$ for all $i \in I$
- Rows J of \mathbf{M} are taken from \mathbf{D} with corresponding potentially non-uniform $\mathbf{h}_J \geq \mathbf{0}$
- \mathbf{B} is uniform on rows J : $\mathbf{B}_j = \gamma < 1$ for all $j \in J$

Then the sum of the source fluxes equal zero, meaning the energy conservation property holds:

$$\mathbf{1}^T \mathbf{Cj} = 0 \quad (80)$$

Proof. The system $\mathbf{Mj} = \mathbf{h}$ yields $\mathbf{C}_I \mathbf{j} = \mathbf{0}$ and $\mathbf{D}_J \mathbf{j} = \mathbf{h}_J$. From Theorem 4.6, it is known that $\mathbf{C}^T (\mathbf{1} - \mathbf{b}) = \mathbf{0}$, which implies $(\mathbf{1} - \mathbf{b})^T \mathbf{Cj} = 0$. Expanding this:

$$(\mathbf{1} - \mathbf{b})^T \mathbf{Cj} = \sum_{i \in I} (1 - \mathbf{b}_i) \mathbf{C}_{i,j} + \sum_{j \in J} (1 - \gamma) \mathbf{C}_{j,j} = 0 \quad (81)$$

The constraint $\mathbf{C}_I \mathbf{j} = \mathbf{0}$ makes the first sum vanish, regardless of the values \mathbf{b}_i . Since $1 - \gamma > 0$, it is obtained that $\sum_{j \in J} \mathbf{C}_{j,j} = 0$. Combined with $\sum_{i \in I} \mathbf{C}_{i,j} = 0$ from $\mathbf{C}_I \mathbf{j} = \mathbf{0}$, this yields $\mathbf{1}^T \mathbf{Cj} = 0$. This establishes energy conservation through the eigenvalue structure, where the mixed constraints create effective uniformity. \blacksquare

6. Numerical Method Validation

For numerical validation, a custom two-dimensional ray tracing code, written by the author with support from artificial intelligence [21], in the Julia programming language [17], was used. This code ray traces in parallel using the central processing unit (CPU), allowing for higher numerical precision than typical graphical processing unit (GPU) ray tracing, and greater data structure flexibility. The code assumes a uniform extinction coefficient β , and ray traces on a coarse mesh, then maps the point of first interaction to a finer mesh, using a grid mapping to find the absorber indices, which allows for efficient ray tracing on arbitrarily fine meshes on the CPU. The code features a custom two-dimensional meshing algorithm which can handle a combination of user-specified skewed quadrilaterals and triangles. Importantly, the rays are traced only until the point of first interaction, as dictated by the proposed transformation. This CPU implementation offers generality, data handling flexibility, code simplicity and code maintainability.

This code also features a Julia adaptation, by permission from the authors, of the MATLAB code by Jacob A. Kerkhoff and Michael J. Wagner, published in their GitHub repository [22], during their work on a paper on solar cavity receivers [23], which implements the three-dimensional analytical view factor method of Narayanaswamy [11].

The Julia CPU code written for validation is available as a registered package for radiative transfer calculations in the Julia programming language [24]. The package is under active development, with documentation and methodology details being continually rolled out at <https://gert.net>.

The hardware used for this validation is a 64-bit PC with an Intel® Core™ i7-14700KF, 3400 MHz, 20 Cores, 28 logical processors CPU and 64 GB of RAM.

6.1. Comparison To The Diffusion Approximation

To compare the proposed transformation to the diffusion approximation, it was applied to a high extinction ($\beta = 100$) non-reflecting non-scattering two-dimensional rectangle of dimensions one thousand meters by one meter. These dimensions were chosen to approximate a one-dimensional problem. Such a one-dimensional problem can be solved using the diffusion approximation for radiative transfer between infinite parallel plates, as described by Howell et al. [4]:

$$\begin{aligned} q_z &= \frac{E_{bw1} - E_{bw2}}{3\beta D/4 + 1/\varepsilon_{w1} + 1/\varepsilon_{w2} - 1} \\ E_{b1} &= E_{bw1} + q_z(1/2 - 1/\varepsilon_{w1}) \\ E_b(z) &= E_{b1} - (3\beta z/4)q_z \end{aligned} \tag{82}$$

where E_{bw1} and E_{bw2} are the area-specific emissive powers of the plates, D is the separation distance and q_z is the area-specific energy transfer rate, E_{b1} is the area-specific emissive power of the medium at the surface of the first wall and $E_b(z)$ is the linearly changing area-specific emissive power of the medium, as a function of position. For the present analysis $E_b(z)$ was normalized by E_{bw1} , and E_{bw2} was set to zero, with $\varepsilon_{w1} = \varepsilon_{w2} = 1$, which simplifies equations (82) to:

$$\frac{E_b(z)}{E_{bw1}} = 1 - \frac{3\beta z/4 + 1/2}{3\beta D/4 + 1} \tag{83}$$

Equation (83) produces a straight line, and for high extinction, the β terms become dominant, and the endpoints are approximately the points (0,1) and (1,0).

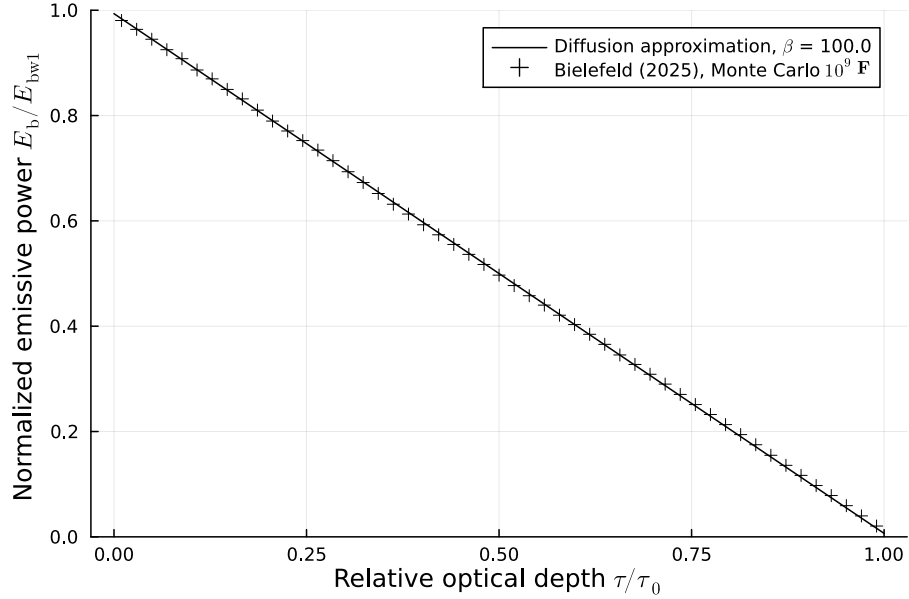


Figure 1: Normalized emissive power along the short centreline in a 1000 m by 1 m geometry (approximately one-dimensional), calculated from the proposed transformation, compared to the diffusion approximation between infinite parallel plates [4]. The medium is absorbing-emitting non-scattering of extinction $\beta = 100$ and the domain has one hot wall, and the remaining non-reflecting non-emitting, all $\varepsilon_w = 1$, with the volume divided into 3×51 elements, and an \mathbf{F} from 10^9 ray samples.

Figure 1 shows the result of application of the proposed transformation, utilizing that $\mathbf{S}_\infty = \mathbf{F}$ meaning $\mathbf{A} = \mathbf{F}$ while $\mathbf{R} = \mathbf{0}$. To compare with equation (83), the following ratio was calculated along the short centre line:

$$\left(\frac{E_b}{E_{bw1}} \right)_i = \frac{e_{g,i}/(4\beta V)}{e_{w1}/A_{w1}} \quad (84)$$

Figure 1 shows equation (83) compared to the results of the proposed transformation, when calculated from equation (84), along the centre line of the short dimension, with an \mathbf{F} produced from sampling 10^9 rays uniformly in a 3×51 domain of dimensions 1000 m by 1 m.

6.2. Comparison to Crosbie and Schrenker

The two-dimensional results of Crosbie and Schrenker [19] are used for validation. Figure 2 was produced by modifying the model of this report by setting gas emissions to zero, since these were neglected by Crosbie and Schrenker, which creates a non-uniform negative source flux in the domain for the absorbing-scattering case. This was achieved by setting the emission probability of gasses in $(\mathbf{1} - \mathbf{B})^T$ (lower blocks) to zero in equations (10) and (11). Table 1 provides an overview of the parameters of the cases used for comparison.

6.3. Comparison to Noble's Formulation of Hottel's Zonal Method

The proposed transformation is compared to Noble's matrix formulation [8] of Hottel's method, which includes the option of solving multiple reflection-scattering problems. This section will show that there exists a subtle discrepancy in Noble's matrix formulation of Hottel's

Table 1: The cases from Crosbie and Schrenker [19] chosen for validation. The parameters describe a square geometry with diffuse radiation incident from one wall. The square has height TAUZ0 and half-width TAUY0, with single scattering albedo of the medium of ALBEDO. NY and NZ refer to the number of quadrature points used in the solution and the emissivity of unity indicates non-reflecting walls.

	Scattering	Absorbing-scattering
TAUY0	0.500	0.500
TAUZ0	1.000	1.000
ALBEDO	1.00	0.50
NY	25	25
NZ	25	25
ε_w	1.00	1.00

method. First it will be shown analytically and next a larger system is solved with the same boundary conditions to validate this conclusion numerically. This discrepancy is not present in the proposed transformation.

6.3.1. Analytical Proof of the Discrepancy

To simplify this derivation, a general constrained geometry is used, with a single surface element and a single enclosed volume element. This geometry satisfies uniform exchange factors $\mathbf{F}_{ss} = \mathbf{F}_{sg} = \mathbf{F}_{gs} = \mathbf{F}_{gg} = 1/2$. Then reciprocity requires $A = 4\beta V$. These requirements might leave additional degrees of freedom, but these are irrelevant for the following derivation. The surface has an emissivity of unity ($\rho = 0$), and the volume has a single scattering albedo of ω .

Application of the Exchange Factor Transformation

After some derivation, for a 2×2 system ($m + n = 2$) with uniform exchange factors, the **A** and **R** matrices of the proposed transformation are given by:

$$\mathbf{A} = \frac{1}{2 - \omega} \begin{bmatrix} 1 & 1 - \omega \\ 1 - \omega & (1 - \omega)^2 \end{bmatrix} \quad (85)$$

$$\mathbf{R} = \frac{1}{2 - \omega} \begin{bmatrix} 0 & \omega \\ 0 & \omega(1 - \omega) \end{bmatrix} \quad (86)$$

And then, after further derivation, **C** and **D** are given by:

$$\mathbf{C} = \frac{1}{2 - \omega} \begin{bmatrix} 1 - \omega & -(1 - \omega) \\ -1 & 1 \end{bmatrix} \quad (87)$$

$$\mathbf{D} = \frac{1}{2 - \omega} \begin{bmatrix} 2 - \omega & 0 \\ -\omega & 2 - 2\omega + \omega^2 \end{bmatrix} \quad (88)$$

Leading to **M** (first row of **D**, second row of **C**):

$$\mathbf{M} = \frac{1}{2 - \omega} \begin{bmatrix} 2 - \omega & 0 \\ -1 & 1 \end{bmatrix} \quad (89)$$

Inverting **M**:

$$\mathbf{M}^{-1} = \begin{bmatrix} 1 & 0 \\ 1 & 2 - \omega \end{bmatrix} \quad (90)$$

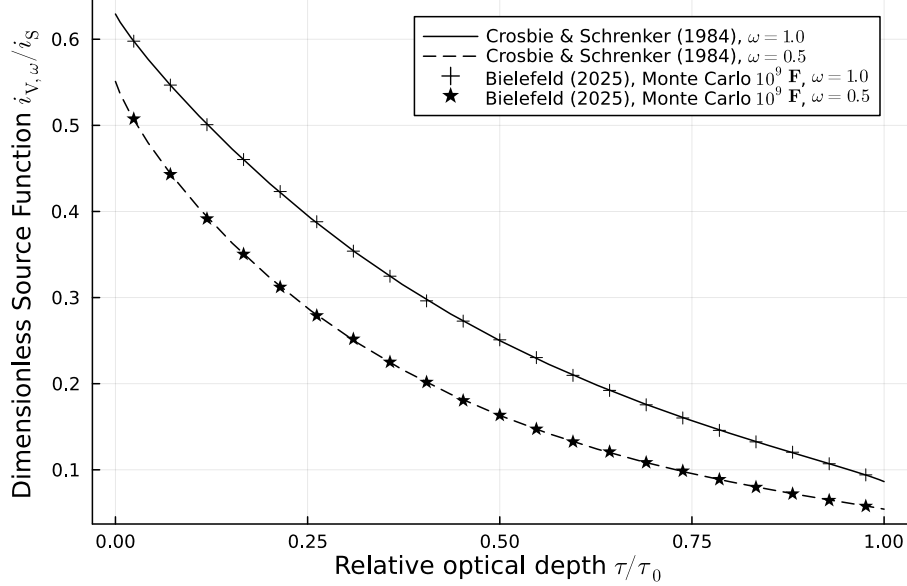


Figure 2: Non-dimensional source function $i_{V,\omega}/i_S$ for the centre line perpendicular to the incident Lambertian intensity onto a two-dimensional square geometry as a function of relative optical depth, based on an estimated \mathbf{F} from ray tracing 10^9 rays in total with no smoothing applied, in a 21×21 geometry, compared to the solutions of Crosbie and Schrenker [19].

Multiplication by a radiative equilibrium boundary condition $\mathbf{h} = [h_1, 0]^T$ yields:

$$\mathbf{j} = \mathbf{M}^{-1}\mathbf{h} = \begin{bmatrix} h_1 \\ h_1 \end{bmatrix} \quad (91)$$

which shows the total radiation is the same for both elements, regardless of ω . Then the total energy balance yields:

$$\mathbf{1}^T \mathbf{Cj} = 0 \quad (92)$$

validating the proposed transformation. Importantly, notice that each element of \mathbf{Cj} is zero individually, as expected. Now to validate against Hottel's method, first the emissive power is calculated from \mathbf{j} , given by:

$$\mathbf{e} = \mathbf{Dj} = \begin{bmatrix} h_1 \\ h_1(1 - \omega) \end{bmatrix} \quad (93)$$

Similarly, the reflected power \mathbf{r} is given by:

$$\mathbf{r} = \mathbf{R}^T \mathbf{j} = \begin{bmatrix} 0 \\ h_1\omega \end{bmatrix} \quad (94)$$

which confirms that ω simply shifts the balance between the scattered power and the emissive power of the volume element, linearly, as expected.

Application of Noble's Formulation of Hottel's Method

Noble's formulation of Hottel's method is applied. Noble's matrices (scalars) here should not be confused with the proposed matrices of this paper, even though some share the same symbols. First the exchange factor matrix is translated to exchange areas by multiplying each row with its corresponding effective area:

$$\mathbf{F}_A = \mathbf{EF} = \begin{bmatrix} \bar{\mathbf{ss}} & \bar{\mathbf{sg}} \\ \bar{\mathbf{gs}} & \bar{\mathbf{gg}} \end{bmatrix} = \begin{bmatrix} A/2 & A/2 \\ 4\beta V/2 & 4\beta V/2 \end{bmatrix} \quad (95)$$

This matrix must be symmetric to satisfy reciprocity, which confirms that $A = 4\beta V$. Using ω and $\rho = 0$ to calculate the intermediate matrices (scalars):

$$\mathbf{P} = [4\beta V \mathbf{I} - \omega \bar{\mathbf{gg}}]^{-1} = \frac{1}{4\beta V - \omega 4\beta V/2} \quad (96)$$

$$\mathbf{L} = \bar{\mathbf{sg}} \mathbf{P} \bar{\mathbf{gs}} = A/2 \frac{1}{4\beta V - \omega 4\beta V/2} 4\beta V/2 = \frac{1}{2} \frac{A}{2 - \omega} \quad (97)$$

$$\mathbf{R} = [A \mathbf{I} - (\bar{\mathbf{ss}} + \omega \mathbf{L}) \rho \mathbf{I}]^{-1} = \frac{1}{A} \quad (98)$$

$$\mathbf{K} = 4\beta \bar{\mathbf{sg}} \mathbf{P} \mathbf{V} \mathbf{I} = 4\beta A/2 \frac{1}{4\beta V - \omega 4\beta V/2} V = \frac{A}{2 - \omega} = 2\mathbf{L} \quad (99)$$

Next, calculating the total exchange areas, according to Noble:

$$\bar{\mathbf{SS}} = \varepsilon \mathbf{AI} \mathbf{R} (\bar{\mathbf{ss}} + \omega \mathbf{L}) \varepsilon \mathbf{I} = A/2 + \frac{\omega}{2} \frac{A}{2 - \omega} \quad (100)$$

$$\bar{\mathbf{SG}} = \bar{\mathbf{GS}}^T = (1 - \omega) \varepsilon \mathbf{AI} \mathbf{R} \mathbf{K} = (1 - \omega) A / (2 - \omega) \quad (101)$$

$$\begin{aligned} \bar{\mathbf{GG}} &= (1 - \omega)^2 4\beta V \mathbf{P} \bar{\mathbf{gg}} + (1 - \omega)^2 \mathbf{K}^T \rho \mathbf{I} \mathbf{R} \mathbf{K} \\ &= (1 - \omega)^2 4\beta V \frac{1}{4\beta V - \omega 4\beta V/2} 4\beta V/2 \\ &= \frac{(1 - \omega)^2 4\beta V}{2 - \omega} \end{aligned} \quad (102)$$

Next, the emissive power solution \mathbf{e} , calculated using the proposed exchange factor transformation is used as an input to Hottel's method, to check whether the two methods agree on energy conservation. This is done by translating \mathbf{e} to specific form, as required by Noble's formulation of Hottel's method, by dividing with the equivalent area of each element:

$$\mathbf{e}_A = \begin{bmatrix} h_1/A \\ h_1(1 - \omega)/(4\beta V) \end{bmatrix} \quad (103)$$

Next, according to Noble, the net source terms of the surface and volume elements are given by:

$$\begin{aligned} \mathbf{Q} &= \varepsilon A \mathbf{E} - \bar{\mathbf{SS}} \mathbf{E} - \bar{\mathbf{SG}} \mathbf{E}_g \\ \mathbf{S} &= \bar{\mathbf{GG}} \mathbf{E}_g + \bar{\mathbf{GS}} \mathbf{E} - (1 - \omega) 4\beta V \mathbf{E}_g \end{aligned} \quad (104)$$

inserting the components of the \mathbf{e}_A -vector and simplifying leads to:

$$\begin{aligned} \mathbf{Q} &= h_1 - \bar{\mathbf{SS}} h_1/A - \bar{\mathbf{SG}} h_1(1 - \omega)/(4\beta V) \\ \mathbf{S} &= \bar{\mathbf{GG}} h_1(1 - \omega)/(4\beta V) + \bar{\mathbf{GS}} h_1/A - (1 - \omega)^2 h_1 \end{aligned} \quad (105)$$

Now, inserting the total exchange areas and simplifying (using $A/(4\beta V) = 1$) yields the following expressions for the normalized net flux of each element:

$$\begin{aligned}\mathbf{Q}/h_1 &= \frac{\omega(1-\omega)}{2-\omega} \\ \mathbf{S}/h_1 &= \frac{\omega(1-\omega)}{2-\omega}\end{aligned}\tag{106}$$

Interestingly, these expressions for the normalized net source terms correspond exactly to the derived gas-gas term of \mathbf{R} of the proposed transformation for the 2×2 case. The expressions of equation (106) are zero only at the extremes of $\omega = 0$ and $\omega = 1$, even though radiative equilibrium was assumed. Since these functions represent net emission and absorption, they always balance due to opposite signs, which ensures overall energy conservation, but simultaneously hides the subtle element-wise discrepancy.

6.3.2. Numerical Validation of the Discrepancy

Figure 3 shows a comparison of the predicted source fluxes in the entire geometry of a 21×21 unit square with constant extinction of $\beta = 1$ and a gas which is in radiative equilibrium with varying single scattering albedo ω . While this geometry differs from the 2×2 analytical case, the boundary condition structure is equivalent: gas in radiative equilibrium (zero source flux) enclosed by surfaces with prescribed emissive power. For this specific case, since the gas is in radiative equilibrium and it is fully enclosed by the surface and the system is in steady state, the net source flux should be zero for both the total surface area and the total gas volume, individually, as was observed for the proposed transformation in the analytical case. Therefore, the total net energy balance of the system should be zero, regardless of the choice of sign for the total surface element and the total volume element. This is the expected behaviour, and furthermore, this behaviour should be independent of the single scattering albedo, due to radiative equilibrium. However, as shown in figure 3, this is not the case for Noble's formulation of Hottel's method, which prescribes signs to this sum to allow cancellation, as predicted analytically. The source flux of the proposed transformation is independent of single scattering albedo, within numerical precision, as expected. Hottel's method only matches the desired behaviour for $\omega = 0$ and $\omega = 1$, and between these values the solution deviates from the analytical accuracy of the proposed transformation. In figure 3, the top crosses with positive source fluxes are the surface elements with incident flux, while the bottom crosses with negative source fluxes are the remaining absorbing surfaces, and the crosses at zero are the gas elements which are in radiative equilibrium. Figure 3 was produced by first solving the mixed boundary problem with incident Lambertian flux onto the unit square geometry in radiative equilibrium using the proposed transformation. Then the source flux distribution of this solution was compared to the source flux distribution of Hottel's method, by using the emissive power distribution from the solution generated with the proposed transformation as an input to Hottel's method. This approach was chosen to avoid tedious entry-wise matrix manipulations to allow for mixed boundary solutions using Hottel's method, and it is the same approach which was used in the analytical derivation. Furthermore, the proposed transformation conserves energy to machine precision for all cases, meaning the sum of all source fluxes in the domain is zero, which is only the case for Hottel's method at the extreme cases of $\omega = 0$ and $\omega = 1$, when the sign convention is disregarded. It was confirmed that, when using the prescribed sign convention, the overall energy balance of Noble's formulation of Hottel's method is indeed approximately equal to zero. To produce the matrix of exchange factors or exchange areas 10^9 rays were traced in total. The shape of the discrepancies

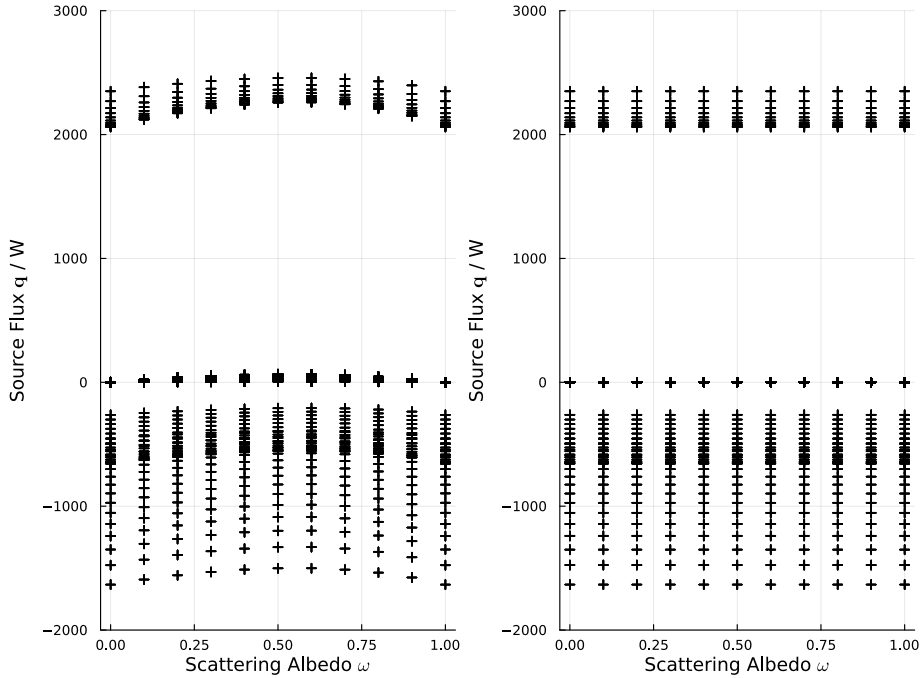


Figure 3: Comparison of Noble's matrix formulation [8] of Hottel's Zonal Method (left) to the proposed exchange factor transformation (right), showing the magnitude of predicted source fluxes of each element in a 21×21 unit square enclosure of a medium in radiative equilibrium with constant extinction $\beta = 1$ and varying albedo ω .

of figure 3 perfectly matches the shape predicted by the analytical expressions of equation (106) which validates the derivation.

6.4. Arbitrary Accuracy

To quantify the accuracy of the proposed transformation, and to show that its accuracy is limited solely by the accuracy of the input exchange factor matrix \mathbf{F} , meaning arbitrary precision can be achieved, the root mean square (RMS) error of the total radiant power was calculated for a total number of ray samples of 10^4 , 10^5 , 10^6 , 10^7 and 10^8 in a non-reflecting non-scattering 21×21 unit square enclosure in radiative equilibrium with incident Lambertian intensity from a surface at 1000 Kelvin. For each of these cases the total radiant power was calculated using the corresponding \mathbf{F} , and the RMS error was calculated:

$$\varepsilon_{\text{RMS}} = \left[\frac{1}{m+n} \sum_{i=1}^{m+n} (\mathbf{j}_i - \mathbf{j}_i^{\text{exact}})^2 \right]^{1/2} \quad (107)$$

where $\mathbf{j}^{\text{exact}}$ was calculated using an exchange factor matrix obtained using 10^{10} ray samples. Figure 4 shows a double-logarithmic plot of the results. The reason for using a 10^{10} ray result as the reference solution instead of the results of Crosbie and Schrenker is to avoid the errors associated with interpolation which would be necessary due to their use of a non-uniform grid, and also to capture the influence of the full domain instead of just part of it.

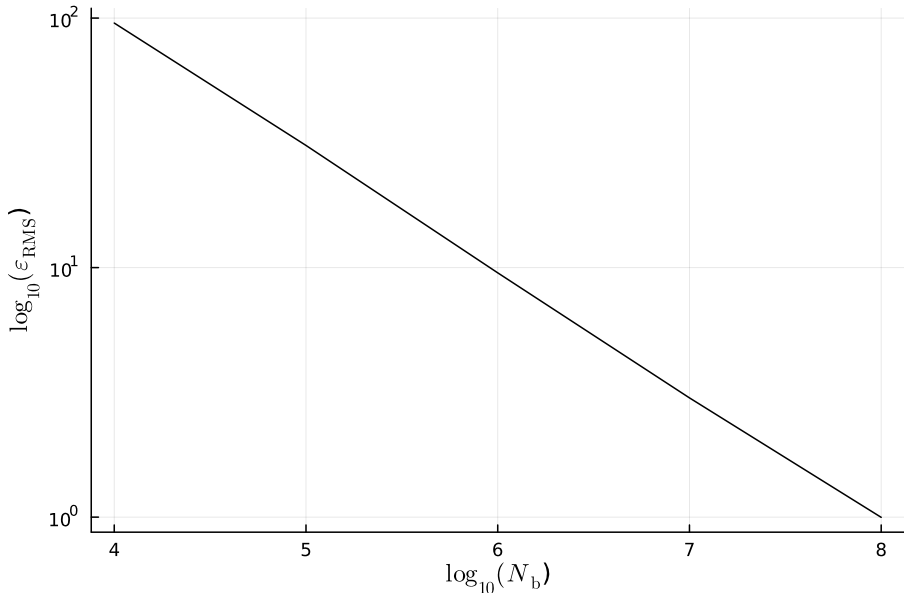


Figure 4: Root mean square error of the total radiant power in a unit square 21×21 enclosure with incident Lambertian intensity onto one side, from an emissive power corresponding to 1000 K, comparing cases with total number of samples of $10^4, 10^5, 10^6, 10^7, 10^8$ to a reference solution obtained using 10^{10} samples.

6.5. Uncertainty Propagation

To quantify how the uncertainty in the exchange factors propagate through the proposed transformation, the following approach was used: First the uncertainty of each entry of the exchange factor matrix was calculated. Since ray tracing is essentially a counting process which follows a Poisson distribution, for a sufficiently large number of trials the distribution of the trials can be modeled as an unbiased normal distribution with a mean value equal to the estimate, and a variance equal to the number of counts [4]. Therefore, the estimate and its standard deviation are given by:

$$\mu_{1-2} = \frac{N_{1-2}}{N_b} \quad , \quad \sigma_{1-2} = \frac{\sqrt{N_{1-2}}}{N_b} \quad (108)$$

where N_{1-2} are the number of bundles emitted by element 1 and absorbed by element 2 and N_b are the total number of bundles emitted by element 1. To calculate how these uncertainties propagate through the solution, the software package *Measurements.jl* [20] for the Julia Programming Language [17] was used, which automatically propagates uncertainties through functionally correlated mathematical operations, including solution of linear systems. The growth or decay of uncertainty from application of the proposed transformation, was quantified by calculating the ratio of the RMS of the relative output uncertainties to the RMS of the relative input uncertainties:

$$r = \frac{(\sigma/\mu)_{\text{RMS,out}}}{(\sigma/\mu)_{\text{RMS,in}}} \quad (109)$$

For the output the total radiant power was used. If the ratio of equation (109) exceed unity, the relative uncertainty has increased, if it is approximately equal to unity, the relative uncertainty is

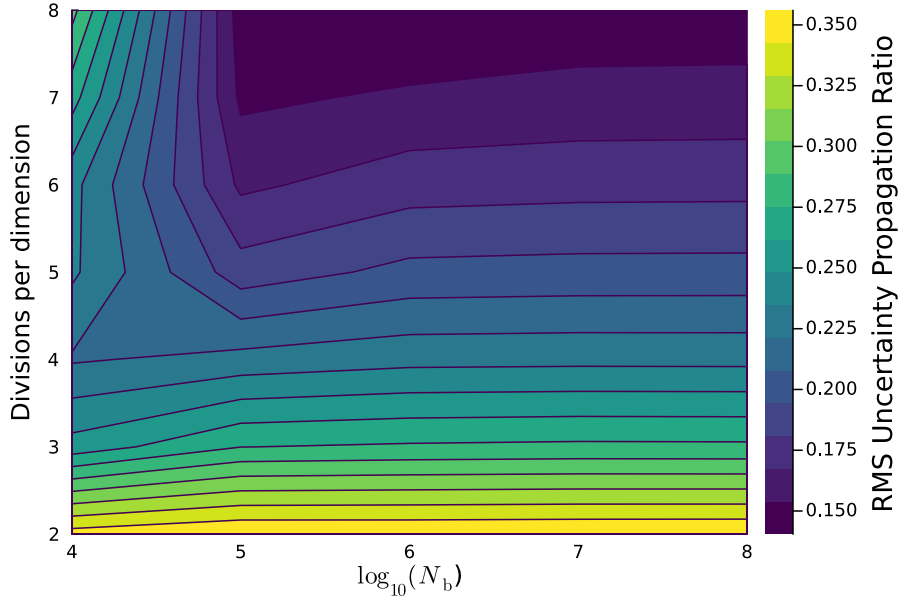


Figure 5: Ratio of RMS relative output uncertainty ($(\sigma/\mu)_{\text{out}}$ (calculated from \mathbf{j}) to RMS relative input uncertainty ($(\sigma/\mu)_{\text{in}}$ (calculated from \mathbf{F}) as a function of the number of ray samples used for obtaining \mathbf{F} (x-axis) and of the number of domain divisions per dimensions (y-axis) in a two-dimensional square geometry. Estimates or results equal to zero were excluded from the calculations.

preserved, and if it is less than unity, the relative uncertainty has decreased. These calculations were performed on non-reflecting non-scattering unit squares in radiative equilibrium with extinction $\beta = 1$, the volume and faces divided according to 2×2 , 3×3 , 4×4 , 5×5 , 6×6 , 7×7 , and 8×8 , leading to exchange factor matrices ranging from dimension 12 to 96. The contour plot of figure 5 shows the result of this calculation, repeating the calculation with 10^4 , 10^5 , 10^6 , 10^7 , 10^8 sample rays for each discretization. The only input uncertainties used in this calculation come from the estimate of \mathbf{F} and estimates or results equal to zero were excluded from the relative uncertainty calculations. From figure 5, since all of the results are well below unity, it can be concluded that application of the proposed transformation significantly decreases the relative uncertainty from the input to the output. This is natural, however, since the largest relative uncertainties come from the smallest exchange factors, which generally affect the results the least. Furthermore, this effect becomes more pronounced with increasing discretization, which is clear from figure 5 from the downward trend in the direction of more domain divisions.

6.6. Range of Applicability

In the proposed transformation, the analytical ray tracing is performed during the inversion of $\mathbf{I} - \mathbf{K}$. To show the limitations of this approach, the following subsections explore the range of applicability of the proposed transformation for three important cases: transparent media, high optical depth media and general participating media.

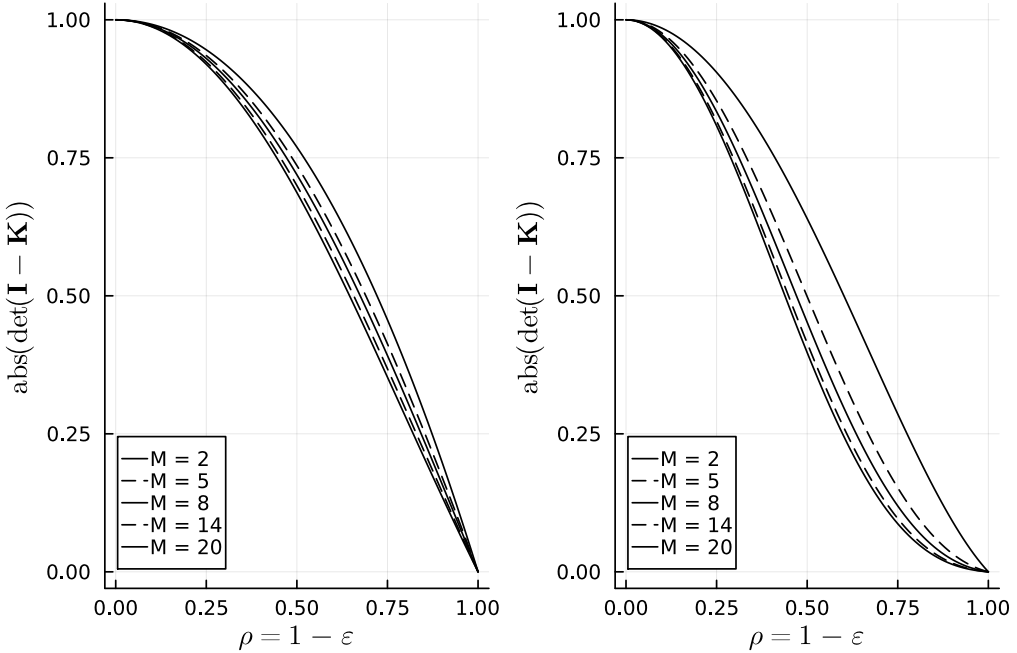


Figure 6: Absolute value of the determinant of $\mathbf{I} - \mathbf{K}$ for a transparent medium in a rectangle of an aspect ratio of unity (left) or an aspect ratio of 10 (right) as a function of uniform reflectivity. The top lines are for $M = 2$ and the lower lines for $M = 20$ and remaining discretizations fall within the bounded region or converge onto the bounds. This figure was created by ray tracing 10^7 rays for each aspect ratio and for each M , with a total of $4M$ wall elements.

6.6.1. Transparent Media

Figure 6 shows the absolute value of the determinant of $\mathbf{I} - \mathbf{K}$ of a transparent rectangular enclosure, as a function of uniform reflectivity in the enclosure, and for two different aspect ratios. The upper and lower lines in the plots ($M = 2$ and $M = 20$) represent the boundaries of the regions, as higher or lower discretizations converge onto these bounds. For $\rho = 0$, the system is perfectly conditioned, and as ρ approaches unity, the conditioning approaches a singularity. This phenomenon occurs earlier with increased discretization and for higher aspect ratio.

6.6.2. Limit of High Optical Depth

To validate the theoretical lower bound on the determinant of $\mathbf{I} - \mathbf{K}$ for uniform reflection-scattering coefficients, as derived in Theorem 3.3 ($\epsilon \leq (1 - b)^{m+n}$), meaning the necessary numerical precision, as a function of albedo and discretization, the analytical bound was compared to the ray tracing results of a square of high optical depth ($\tau = 10^3$). Figure 7 compares the calculated analytical bound to the results obtained by ray tracing 10^7 rays in varying levels of discretization, for different levels of uniform scattering coefficients, by calculating the absolute value of the determinant of $\mathbf{I} - \mathbf{K}$. In the limit of high optical depth, the bound accurately captures the lower bound of the necessary numerical precision (truncated to 256-bit precision), and can thus serve as a simple guiding principle for application of the proposed transformation. This bound is only accurate for high optical depths, since at lower optical depths $\mathbf{I} - \mathbf{K}$ is generally

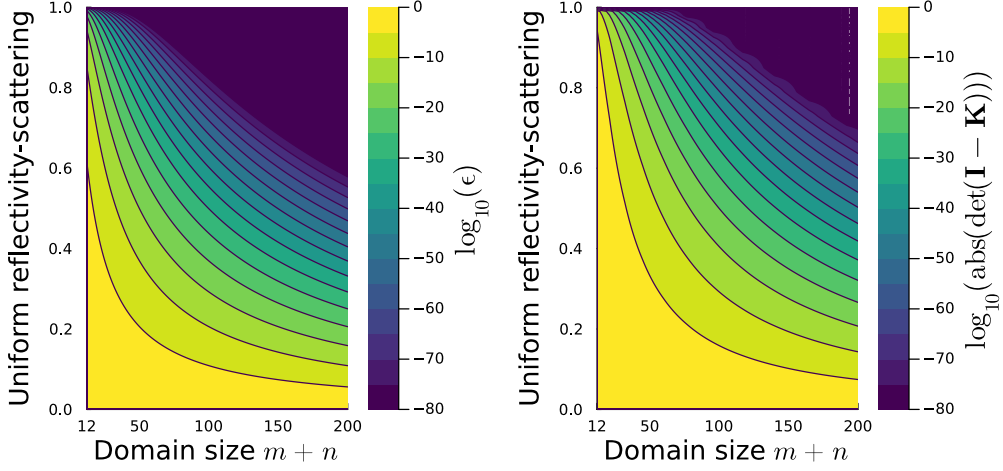


Figure 7: Application of Theorem 3.3 ($\epsilon \leq (1 - b)^{m+n}$) to calculate the theoretical lower bound on the determinant (left), compared to the absolute value of the determinant of $\mathbf{I} - \mathbf{K}$ for a two-dimensional square of uniform reflection-scattering coefficient and high optical depth ($\tau = 10^3$), from ray tracing 10^7 rays per domain size (right).

non-singular, since it approaches the transparent limit (section 6.6.1).

6.6.3. General Participating Media

Figure 8 shows four contour plots of the absolute value of the determinant of $\mathbf{I} - \mathbf{K}$ for a two-dimensional square enclosure, indicating the required numerical precision for a range of different problem configurations. To include a large range, figure 8 is triple logarithmic, and the parameter space is the number of subdivisions M along each wall of the square enclosure ($m + n = 4M + M^2$ where $m + n$ is the number of elements), the optical depth τ along a wall, and single scattering albedo ω . For $\omega = 0$, the proposed transformation has perfect conditioning for the entire parameter space since $\mathbf{S}_\infty = \mathbf{F}$. For $\omega > 0$, with high extinction and for highly discretized domains, a region of computational infeasibility begins to form, where numerical precision beyond 256-bit would be required (this region was truncated in figure 8). As ω approaches unity, this region increases in size, clearly limiting the range of applicability of the proposed transformation. To solve problems with a combination of high optical depth and high scattering, the domain should be coarsely discretized, while on the other hand, to solve highly discretized domains, the optical thickness should be low. Figure 8 was produced based on calculation of the absolute value of the product of the eigenvalues of $\mathbf{I} - \mathbf{K}$ for a range of different \mathbf{F} , found from ray tracing 10^6 rays for each combination of M and τ .

6.7. Application to a Complex Geometry

Figure 9 shows the result of applying the proposed transformation to a non-reflecting non-scattering complex star-shaped geometry with volumetric in-flux of energy. This class of problems with distributed volumetric energy sources is fundamental to the analysis of combustion chambers, furnace design, and other high-temperature industrial applications where radiative heat transfer governs thermal behavior. The star-shaped geometry was chosen to simultaneously

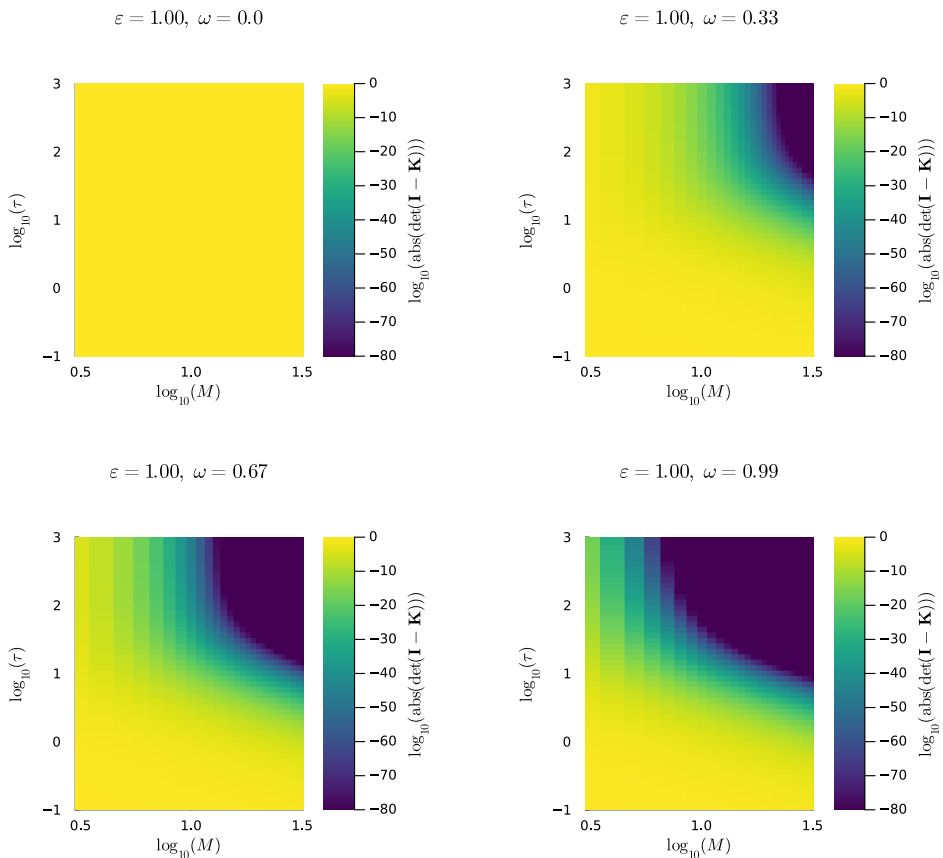


Figure 8: Absolute value of the determinant of $\mathbf{I} - \mathbf{K}$ for a two-dimensional square with absorbing walls and a grid from M subdivisions along each wall and optical depth τ along each wall for four different uniform values of single scattering albedo, from ray tracing 10^6 rays uniformly in total in each grid.

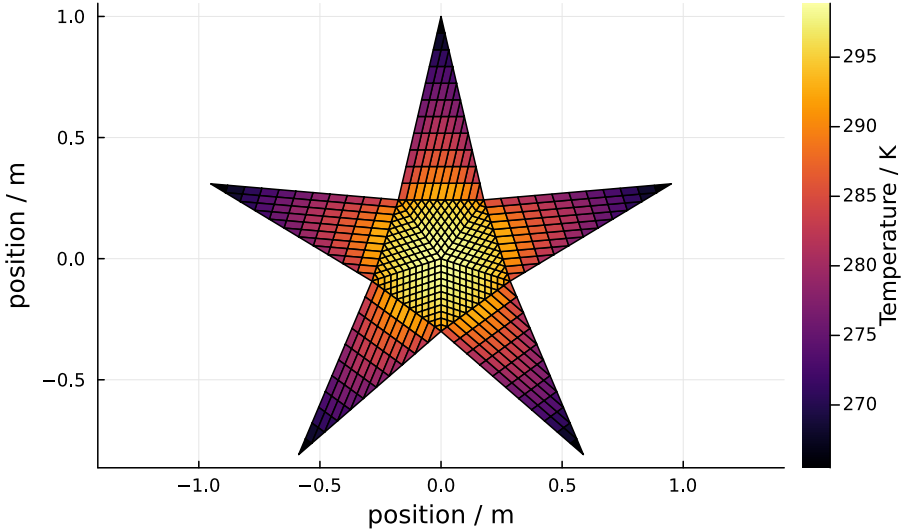


Figure 9: Solution of a non-reflecting non-scattering complex star-shaped geometry with volumetric in-flux of energy. Each overall triangle has a uniform positive source in-flux of 1 kW per triangle. The arms have fully absorbing boundaries at zero Kelvin.

assess the method's performance in geometrically complex scenarios. The inner pentagon is assembled from 5 triangles with all sides transparent, while the arms of the star are impenetrable on the outside and transparent towards the central pentagon. The outer impenetrable boundaries of the arms are set to fully absorbing at a temperature of zero Kelvin. The medium in each overall triangle has a uniform source in-flux of 1 kW per triangle giving 10 kW in-flux in total. The participating medium has unity extinction and is absorbing-emitting non-scattering. The temperature field of the solution of figure 9 displays the expected symmetry and cooling of the medium towards the tips of the arms. At the corners of the pentagon the temperature is slightly lower than at the center, due to cooling from the adjacent walls. It is concluded that a complex geometry does not complicate application of the proposed transform, but rather increases the complexity demand imposed on the ray tracing algorithm used for obtaining \mathbf{F} .

6.8. Application to a Transparent Three-Dimensional Problem

Figure 10 shows the proposed transformation applied to a non-reflecting three-dimensional unit cube vacuum enclosure, meaning a fully transparent medium. In this case one can entirely neglect the \mathbf{F}_{sg} , \mathbf{F}_{gs} and \mathbf{F}_{gg} matrix blocks and focus solely on the \mathbf{F}_{ss} block, validating that the method applies equally to transparent and participating media. The proposed exchange factor transformation operates as a graph equilibrium algorithm, working solely with probabilities and transfer rates of a conserved quantity. This mathematical generality, rooted in graph theory principles, enables the method to handle diverse geometric configurations and suggests potential applications beyond radiative heat transfer. Its foundational character stems from this abstraction to probabilistic transfers on a network, which maintains validity regardless of the specific

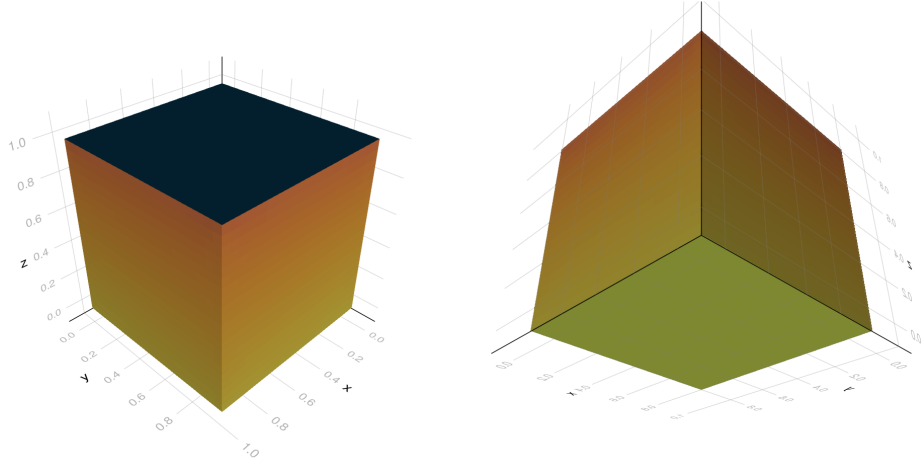


Figure 10: Temperature field solution of a transparent three-dimensional problem. The top face has a prescribed temperature of zero Kelvin and the bottom face has a prescribed temperature of 1000 Kelvin. The vertical faces have a prescribed source flux of zero. Each face consists of 21×21 squares, each decomposed into two triangles for plotting. Each triangle has been coloured according to the temperature of its square with no interpolation applied. The view factor matrix was obtained using the method of Narayanaswamy [11].

physical interpretation of the nodes and connections. This is the reason that neglecting the gas parts of \mathbf{F} does not affect the validity of the solution. In figure 10, each face consists of 21×21 subsurfaces and the top cold face has a fixed temperature of zero Kelvin while the bottom hot surface has a fixed temperature of 1000 Kelvin. The vertical faces have a prescribed source flux of zero, meaning they are entirely re-radiating. The three-dimensional plot serves as a qualitative validation and shows the expected resulting temperature gradient across the vertical faces. To create figure 10 the view factor matrix was obtained using the method of Narayanaswamy [11] and no interpolation was applied when rendering the figure.

6.9. Application To a Medium-Scale Problem

To demonstrate that the proposed transformation is applicable to general medium-scale problems, it was applied to a two-dimensional unit square geometry with $\beta = 1$ and 151 splits in both dimensions. This yields a dense exchange factor matrix of dimension $4 \cdot 151 + 151^2 = 23405$, meaning all of the remaining matrices will be of this size. For demonstration, 10^9 ray samples were traced in parallel using CPU multi-threading in this geometry. The ray tracing took 15 minutes and 20 seconds. Subsequent application of the proposed transformation to a problem with an absorbing-emitting medium in radiative equilibrium with $\kappa = 1$ and $\sigma_s = 0$, including all of the necessary matrix operations, took 75 seconds, using Julia's built-in backslash operator [17] for the matrix linear solve for \mathbf{S}_∞ and using Intel's Math Kernel Library (MKL) LU Factorization [27] with relative and absolute tolerances of 10^{-12} for the final vector linear solve for \mathbf{j} . Figure 11 shows the results, comparing the solution to the pure scattering results of Crosbie and Schrenker [19] (Table 1). Solving the same problem, but instead with $\sigma_s = 1$ and $\kappa = 0$, took 140 seconds, and did not require additional ray tracing since β was unchanged, and yielded an identical result in terms of the non-dimensional source function. This fact, that the dimensionless source

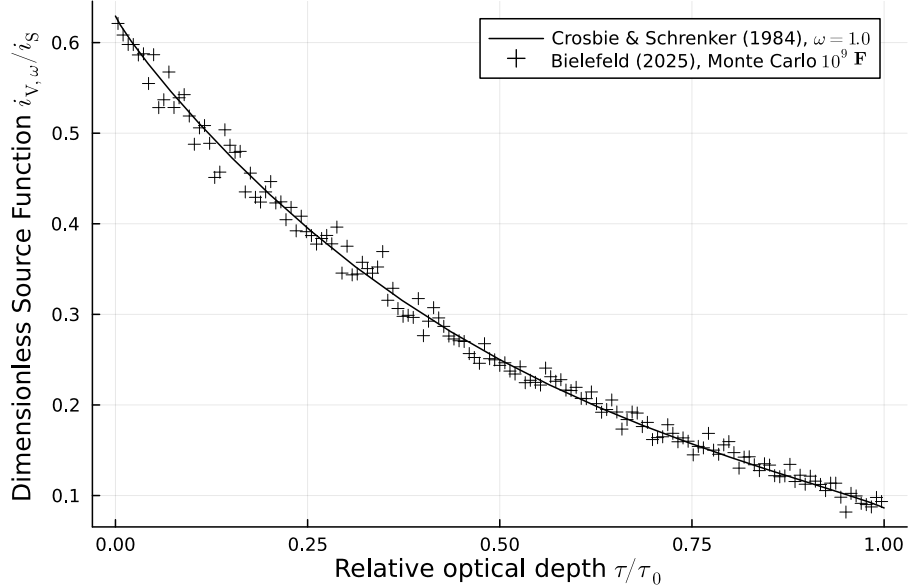


Figure 11: Comparison of the centreline dimensionless source function perpendicular to incident radiation. Crosses show the results of application of the proposed transformation to a 151×151 square two-dimensional either absorbing-emitting ($\kappa = 1, \sigma_s = 0$) or scattering ($\kappa = 0, \sigma_s = 1$) medium in radiative equilibrium and $\beta = 1$, using an \mathbf{F} obtained from 10^9 ray samples, while the solid line shows the results of Crosbie and Schrenker in a purely scattering medium ($\kappa = 0, \sigma_s = 1$).

function is identical for an absorbing-emitting medium in radiative equilibrium and a scattering medium, further validates the internal consistency of the proposed transformation.

7. Discussion

7.1. Scalability Assessment

In its basic form, the proposed transformation is limited to medium-scale problems, for general problems involving reflection-scattering. The primary limitation is one of memory, as the dimension of all matrices involved in the proposed transformation is equal to the number of elements. This clearly prohibits what is possible on a regular personal computer. On a high performance computing cluster more memory is typically available, which will allow for larger matrices. Furthermore, the option of using storage disk space to supplement the computer working memory may be utilized to broaden the number of problems which can be solved, even though this will increase the time demand. For high extinction problems, \mathbf{F} will be sparse, but the remaining matrices of the proposed transformation will in general be non-sparse for reflecting-scattering problems. For high extinction problems with negligible reflection-scattering, the proposed method should be applicable to large-scale problems, since this avoids the dense matrices arising from reflection-scattering. However, this will require sparse matrix memory storage, as well as linear solvers which support sparse matrix data structures.

Numerical precision limitations depend on the structure of \mathbf{F} . While the row-stochastic constraint requires entries to sum to unity, radiation exchange factors are typically localized: nearby

elements exchange more than distant ones, giving \mathbf{F} a sparse or diagonally-dominant structure even for moderate extinction. This natural structure keeps individual entries well above machine precision for practical problem sizes. The primary limitation for dense reflecting-scattering problems remains memory: storing and operating on $(m + n)^2$ dense matrices becomes prohibitive before precision limits are reached. For GPU ray tracing using 32-bit precision, the reduced machine epsilon of approximately $1.19 \cdot 10^{-7}$ may require attention for highly discretized domains with near-uniform exchange factors, suggesting 64-bit precision for such cases.

7.2. Computational Complexity

For larger problems, the computational complexity of the proposed transformation is dominated by the linear solves for \mathbf{S}_∞ and \mathbf{j} . Since \mathbf{S}_∞ is a matrix, its computation effectively involves $m + n$ linear problems, while \mathbf{j} requires only a single vector linear solve. As shown in Theorem 3.3, this computational burden varies by domain type: For an absorbing-emitting non-reflecting non-scattering domain, the computation of $(\mathbf{I} - \mathbf{K})^{-1}$ becomes trivial, resulting in $\mathbf{S}_\infty = \mathbf{F}$ (since $\mathbf{B} = \mathbf{K} = \mathbf{0}$), while for a reflecting-scattering domain, the full set of linear problems must be solved for \mathbf{S}_∞ . However, the results of section 6.9 demonstrate an execution time ratio of less than 2 \times , between two such problems of significantly different difficulty level. Considering equations (10) and (11) for \mathbf{A} and \mathbf{R} , this balance in complexity can be explained: For the absorbing-emitting case, the complexity of the algorithm is primarily due to the solve for \mathbf{j} , since $\mathbf{S}_\infty = \mathbf{F}$. As the system becomes more reflecting and scattering, the solve for \mathbf{S}_∞ begins to dominate, but simultaneously the solve for \mathbf{j} becomes increasingly tractable due to increased sparsity of \mathbf{M} , due to the multiplications with $(\mathbf{I} - \mathbf{B})^T$ and $(\mathbf{I} - \mathbf{B})$ in the equations for \mathbf{A} and \mathbf{R} , and in the limit of a perfectly reflecting-scattering domain ($\mathbf{B} = \mathbf{1}$), $\mathbf{A} = \mathbf{0}$ and $\mathbf{R} = \mathbf{0}$ and $\mathbf{M} = \mathbf{I}$ and the linear solve vanishes such that $\mathbf{j} = \mathbf{h}$. The least computationally complex case appears when all temperatures are known ($\mathbf{M} = \mathbf{D}$) and in the absence of reflection-scattering ($\mathbf{B} = \mathbf{0}$, $\mathbf{A} = \mathbf{S}_\infty = \mathbf{F}$, $\mathbf{R} = \mathbf{0}$ and $\mathbf{D} = \mathbf{I}$), where both of the linear solves vanish, so that $\mathbf{j} = \mathbf{h}$, making this case computationally ideal for dynamic time simulation, as long as photon time-of-flight effects can be neglected.

7.3. Comparison to Existing Methods

Advantages of the proposed transformation include flexibility through ray tracing for \mathbf{F} , allowing for modelling of relevant phenomena. The proposed transformation is a general unifying framework in terms of both extinction and reflection-scattering, applicable to the full range of reflection and scattering as well as extinction, from transparent to optically thick media. It is applicable to any geometry and, after ray tracing, any number of problems with the same level of extinction may be solved without further ray tracing. The method has guaranteed convergence properties and physical correctness. As demonstrated in section 6.3, the proposed transformation provides improved accuracy for intermediate scattering ranges when compared to Hottel's method, while section 6.2 shows that the proposed transformation agrees with the work of Crosbie and Schrenker in the same albedo range, while at the same time being more flexible and general than their methodology.

Other methods, such as moment-based methods, spherical harmonics, discrete ordinates, and finite element methods are inherently non-analytical numerical approximations, since they depend on some form of truncation, either of a series of equations which is in reality infinite, or by the use of a finite set of discrete angles, to describe a continuum of angles. The proposed transformation does not resort to any such truncation, apart from the spatial discretization of the domain into finite elements. As shown in Theorem 3.1, the Neumann series analytically traces

all multiple reflection-scattering paths to their endpoints exactly. The proposed method either succeeds with machine-precision accuracy or fails when numerical precision is insufficient.

The transformation itself is fully analytical: given an exact \mathbf{F} , all subsequent operations yield exact results. This enables symbolic solutions for small systems, as demonstrated in section 6.3, though complexity grows rapidly with system size due to the two linear solves required. For participating media, \mathbf{F} is typically estimated via Monte Carlo and thus approximate, so the overall solution accuracy is bounded by the accuracy of \mathbf{F} . However, the framework introduces no additional approximation error beyond what is present in \mathbf{F} .

The proposed transformation may be viewed as an augmented form of Monte Carlo. For highly reflecting-scattering domains, such as clouds or snow, the analytical path tracing significantly outperforms basic Monte Carlo methods. The timings in section 6.9 illustrate this: ray tracing 10^9 first-interaction rays required 15 minutes, while the subsequent matrix solve took at most 140 seconds. Conventional Monte Carlo for pure scattering ($\omega = 1$) would require tracing each ray through numerous scattering events: the expected path length grows without bound as $\omega \rightarrow 1$, multiplying the ray tracing cost accordingly. The proposed method instead traces rays only to first interaction, then analytically resolves all subsequent scattering through the matrix framework. Additionally, once \mathbf{F} is computed, problems with different combinations of κ and σ_s summing to the same β can be solved without further ray tracing, enabling rapid parameter studies.

Furthermore, the simplified first-interaction ray tracing provides a more accessible pathway to the programming of radiative transfer solvers, while simultaneously making the ray tracing highly suitable for both CPU and GPU parallel execution. Unlike conventional multiple scattering ray tracing, where rays terminate after unpredictable numbers of bounces creating workload imbalance, first-interaction tracing has predictable and uniform workload per ray. This also provides a validation pathway for developers of new Monte Carlo solvers: by implementing first-interaction tracing and applying the proposed transformation, one obtains exact multiple reflection-scattering solutions that can serve as reference benchmarks for validating full Monte Carlo implementations on arbitrary geometries.

7.4. Limitations and Future Work

Limitations of the proposed transformation include the general need for ray tracing. While Monte Carlo ray tracing can achieve arbitrary accuracy with quantifiable bounds, its convergence rate is proportional to $N_b^{-1/2}$, meaning high ray sample counts are preferred. To preserve accuracy under increased discretization the number of ray samples per cell should remain constant. For high resolution domains with several elements, this leads to an unfortunate scaling of the total necessary ray bundles, as evident from the random noise of figure 10. Therefore, to harness the full potential of the proposed transformation, when applied to larger problems, some form of variance reduction should be applied. The non-linear optimization-based exchange factor smoothing algorithms commonly encountered in the literature, while theoretically capable of addressing problems of this structure, face significant practical limitations as problem size increases, and at the scale of figure 10, with an \mathbf{F} having more than half a billion matrix entries, even proprietary solvers encounter computational bottlenecks including memory constraints, numerical instability, and diminishing convergence rates. Therefore, novel and efficient algorithms for exchange factor smoothing are needed, which remain computationally tractable for high resolution domains.

The major limitation of the proposed transformation is that it is not applicable to general large-scale problems, due to the scaling of dense matrices. However, to apply the proposed

transformation to such problems, it might be possible to apply some form of domain decomposition, followed by sequential iterative solution where the boundary fluxes should match between decomposed parts. The proposed transformation lends itself naturally to this type of decomposition, since discrete angular in-flux information can be obtained from the entries of the entry-wise product $(\mathbf{A}^T + \mathbf{R}^T)_i \circ \mathbf{j}$, where the index i denotes the row, meaning this vector gives the in-flux of power onto row element i from each column element j in the domain. A general algorithm for accomplishing such a decomposed solution would be a valuable extension of the proposed transformation.

If one has a priori knowledge of the problem to be solved, one may sample the domain selectively for \mathbf{F} , for example based on the emissive power for non-reflecting non-scattering problems, or based on the previous \mathbf{j} for general dynamic problems, rather than the uniform sampling which was used in this paper. This could potentially allow a significant reduction in the number of samples necessary to accurately resolve the radiative transfer field. This importance sampling would be especially relevant for dynamic problems, where \mathbf{F} needs to be updated for each time step, for example for convective transport of a fluid with spatially and temporally varying extinction β .

The proposed transformation is not yet applicable to varying angular distributions of emission and reflection-scattering, since these are fixed from the ray tracing distributions used to obtain \mathbf{F} (uniform for volumes and Lambertian for surfaces in this paper). A method to include such behaviour into the proposed transformation would be valuable and could broaden its applicability and generality.

The proposed transformation is a grey approximation and is not yet applicable to spectral problems, limiting the applicability to real-world problems.

8. Conclusion

This paper introduced an exchange factor transformation as a matrix-based technique with proven properties for solving coupled mixed boundary condition radiative transfer problems. By transforming the first interaction-based exchange factor matrix into absorption and multiple reflection-scattering matrices through analytical path tracing, the method provides guaranteed convergence, energy conservation to working numerical precision, and non-negative radiation results under specified conditions: properties that are proven rather than merely empirical.

The method shows excellent agreement with the diffusion approximation and established reference work by Crosbie and Schrenker, while the comparison with Noble's formulation of Hottel's method revealed a previously unidentified discrepancy at intermediate scattering albedos. The analytical nature of the transformation enables exact solutions for reflecting-scattering problems within its domain of applicability. Its effectiveness spans the complete range from transparent to optically thick participating media with varying boundary conditions. The framework offers computational efficiency for medium-scale general reflecting-scattering problems and scales to large problems when negligible reflection-scattering and high extinction ensure matrix sparsity.

Conflict Of Interest

The author acknowledges previous employment as an intern at the boiler and power plant company Aalborg Energie Technik A/S during autumn 2022, while completing the 9th semester

of his Master's in Thermal Energy and Process Engineering at Aalborg University, and current employment at the engineering consulting firm Added Values P/S. This research was conducted independently, outside of regular work hours, and without financial or material support from either organization. The views and conclusions presented in this paper represent the author's personal work and do not necessarily reflect the positions or policies of the aforementioned employers.

Funding

This research did not receive any specific grant from funding agencies in the public, commercial, or not-for-profit sectors.

Declaration of generative AI and AI-assisted technologies in the writing process

During the preparation of this work the author used Anthropic's Claude Sonnet 3.5 [21] and later Claude Sonnet 4.0. These models provided invaluable assistance, which supported all stages of this research, from method development through manuscript preparation. In particular, Claude Sonnet 3.5 facilitated iterative development and refinement of key concepts and arguments, which led to the fundamental breakthrough during the summer of 2024. Claude Sonnet 4.0 assisted in formulating the proofs of physical correctness. Claude Opus 4.5 assisted with final manuscript review and language refinement. After using these tools/services, the author reviewed and edited the content as needed and takes full responsibility for the content of the published article.

Acknowledgements

The author wishes to acknowledge the following assistance: His friends Snorre Marstrand Enevoldsen and Sune Borkfelt who helped by proof reading the English language of the draft manuscript. The author's former supervisors at Aalborg University, Thomas Joseph Condra and Kim Sørensen, as well as the author's current colleague Gorm Bruun Andresen who all helped by proof reading the English language of the draft manuscripts and by suggesting improvements to the presentation. The financial support from the author's parents during his education.

An earlier version of this manuscript was submitted to a peer-reviewed journal. The author is grateful to the anonymous reviewers whose thoughtful feedback and constructive suggestions substantially strengthened this work, leading to a more comprehensive validation framework and enhanced comparison to existing methods.

Software

All calculations were performed using the Julia programming language [17]. The two-dimensional figures were created using the Julia package Plots.jl [26] and the three-dimensional figure was rendered using the Julia package Makie.jl [25].

References

- [1] Kirchhoff, G., *Ueber das Verhältniss zwischen dem Emissionsvermögen und dem Absorptionsvermögen der Körper für Wärme und Licht*, Annalen der Physik und Chemie, 109, 275-301, 1860.
- [2] Schwarzschild, K., *Ueber das Gleichgewicht der Sonnenatmosphäre*, Nachrichten von der Gesellschaft der Wissenschaften zu Göttingen, Mathematisch-Physikalische Klasse, 1906, 41-53, 1906.
- [3] Chandrasekhar, S., *Radiative Transfer*, Clarendon Press, Oxford, International Series of Monographs on Physics, 1950.
- [4] Howell, J. R. and Mengüç, M. P. and Daun, K. J. and Siegel, R., *Thermal Radiation Heat Transfer*, CRC Press, Taylor & Francis Group, 7th edition, 2021.
- [5] Modest, M. F. and Mazumder, S., *Radiative Heat Transfer*, Academic Press, 4th edition, 2022.
- [6] Hottel, H. C. and Cohen, E. S., *Radiant Heat Exchange In A Gas-Filled Enclosure: Allowance For Nonuniformity Of Gas Temperature*, A.I.Ch.E., Vol. 4, No. 1, March, 1958.
- [7] Hottel, H. C. and Sarofim, A. F., *Radiative Transfer*, McGraw-Hill Book Company, 1st edition, 1967.
- [8] Noble, J. J., *The Zone Method: Explicit Matrix Relations For Total Exchange Areas* Int. J. Heat Mass Transfer., Vol 18, pp. 261-269, 1975.
- [9] Metropolis, N. and Ulam, S., *The Monte Carlo Method*, J. Am. Stat. Assoc., 44(247), pp. 335-341, September, 1949.
- [10] Beckman, W. A., *Temperature Uncertainties In Systems With Combined Radiation And Conduction Heat Transfer*, ASME, Aviation & Aerospace Conference, June, 1968.
- [11] Narayanaswamy, A., *An Analytic Expression For Radiation View Factor Between Two Arbitrarily Oriented Planar Polygons*, International Journal of Heat and Mass Transfer 91 (2015) 841–847.
- [12] Minkowycz, W. J. and Sparrow, E. M. and Schneider, G. E. and Pletcher, R. H., *Handbook of Numerical Heat Transfer*, John Wiley & Sons, Inc., 1988.
- [13] Daun, K. J. and Morton, D. P. and Howell, J. R., *Smoothing Monte Carlo Exchange Factors Through Constrained Maximum Likelihood Estimation*, ASME Journal of Heat Transfer, October, 2005.
- [14] Born, M. and Wolf, E., *Principles of Optics - Electromagnetic Theory of Propagation, Interference and Diffraction of Light* Pergamon Press, Sixth (corrected) edition, 1980.
- [15] Howell, J. R and Daun, K. J., *The Past and Future of the Monte Carlo Method in Thermal Radiation Transfer* ASME Journal of Heat Transfer, Vol. 143, October 2021.
- [16] IEEE Standard for Floating-Point Arithmetic, IEEE Std 754-2019 (Revision of IEEE 754-2008), pp. 1-84, 2019.

- [17] Bezanson, J. and Edelman A. and Karpinski, S., and Shah, V. B. *Julia: A Fresh Approach to Numerical Computing* SIAM Review. Vol. 59, Iss. 1 (2017).
- [18] Horn, R. A. and Johnson, C. R., *Matrix Analysis*, Cambridge University Press, 2nd edition, 2018.
- [19] Crosbie, A. L. and Schrenker, R. G., *Radiative Transfer In A Two-Dimensional Rectangular Medium Exposed To Diffuse Radiation* J. Quant. Spectrosc. Radiat. Transfer, Vol. 31, No. 4, pp. 339-372, 1984.
- [20] Giordano, M., *Uncertainty Propagation With Functionally Correlated Quantities* Preprint 28 October 2016.
- [21] Anthropic, 2024, *Claude 3.5 Sonnet*, <https://www.anthropic.com/news/clause-3-5-sonnet>.
- [22] Kerkhoff, J. A. and Wagner, M. J., *viewFactor.m*, <https://github.com/uw-esolab/docs/tree/main/tools/viewfactor> Energy Systems Optimization Lab, University of Wisconsin–Madison.
- [23] Kerkhoff, J. A. and Wagner, M. J., *A Flexible Thermal Model for Solar Cavity Receivers Using Analytical View Factors*, ASME Energy Sustainability Proceedings, July 22, 2021.
- [24] Bielefeld, N. M., *RayTraceHeatTransfer.jl*, <https://github.com/NikoBiele/RayTraceHeatTransfer.jl>, July, 2024.
- [25] Danisch, S. and Krumbiegel, J., *Makie.jl: Flexible high-performance data visualization for Julia*, Journal of Open Source Software, The Open Journal, Vol. 6, no. 65, pp. 3349, 2021.
- [26] Christ, S. and Schwabeneder, D. and Rackauckas, C. and Borregaard, M. K. and Breloff, T., *Plots.jl – a user extendable plotting API for the julia programming language*, Journal of Open Research Software, 2023.
- [27] *Developer Reference for Intel® oneAPI Math Kernel Library for C*, <https://www.intel.com/content/www/us/en/docs/onemkl/developer-reference-c/2025-0/overview.html>, Intel®, 2025.